Appl Microbiol Biotechnol (2016) 100:7957–7976
DOI 10.1007/s00253-016-7576-7

Community proteomics provides functional insight into polyhydroxyalkanoate production by a mixed microbial culture cultivated on fermented dairy manure

Andrea J. Hanson[1] · **Nicholas M. Guho**[2] · **Andrzej J. Paszczynski**[3] · **Erik R. Coats**[2]

Received: 5 March 2016 / Revised: 15 April 2016 / Accepted: 21 April 2016 / Published online: 5 May 2016

Abstract Polyhydroxyalkanoates (PHAs) are bio-based, biodegradable polyesters that can be produced from organic-rich waste streams using mixed microbial cultures (MMCs). To maximize PHA production, MMCs are enriched for bacteria with a high polymer storage capacity through the application of aerobic dynamic feeding (ADF) in a sequencing batch reactor (SBR), which consequently induces a feast-famine metabolic response. Though the feast-famine response is generally understood empirically at a macro-level, the molecular level is less refined. The objective of this study was to investigate the microbial community composition and proteome profile of an enriched MMC cultivated on fermented dairy manure. The enriched MMC exhibited a feast-famine response and was capable of producing up to 40 % (wt. basis) PHA in a fed-batch reactor. High-throughput 16S rRNA gene sequencing revealed a microbial community dominated by *Meganema*, a known PHA-producing genus not often observed in high abundance in enrichment SBRs. The application of the proteomic methods two-dimensional electrophoresis and LC-MS/MS revealed PHA synthesis, energy generation, and protein synthesis prominently occurring during the feast phase, corroborating bulk solution variable observations and theoretical expectations. During the famine phase, nutrient transport, acyl-CoA metabolism, additional energy generation, and housekeeping functions were more pronounced, informing previously under-determined MMC functionality under famine conditions. During fed-batch PHA production, acetyl-CoA acetyltransferase and PHA granule-bound phasin proteins were in increased abundance relative to the SBR, supporting the higher PHA content observed. Collectively, the results provide unique microbial community structural and functional insight into feast-famine PHA production from waste feedstocks using MMCs.

Keywords Aerobic dynamic feeding (ADF) · Feast-famine response · Polyhydroxyalkanoates (PHAs) · Volatile fatty acids (VFAs) · Gel-based microbial community proteomics · LC-MS/MS · Illumina sequencing

Introduction

Polyhydroxyalkanoates (PHAs) are linear polyesters synthesized by bacteria that can functionally replace many conventional petroleum-based plastics (Keshavarz and Roy 2010). Current PHA production practices generally rely on pure microbial cultures cultivated under axenic conditions and fed synthetic, food-based substrate (i.e., corn sugar) (DiGregorio 2009). To expand commercial PHA production while concurrently reducing the environmental footprint and production costs, the use of mixed microbial cultures (MMCs) and inexpensive waste feedstocks of agricultural or industrial origin has been proposed (Dias et al. 2006; Serafim et al. 2008). For this approach to be successful, MMCs must first be enriched for PHA-producing bacteria with high PHA storage capacity. Once MMCs are physiologically conditioned for polymer accumulation, a portion of the culture is used to

Electronic supplementary material The online version of this article (doi:10.1007/s00253-016-7576-7) contains supplementary material, which is available to authorized users.

✉ Erik R. Coats
ecoats@uidaho.edu

[1] Department of Biological Sciences, University of Idaho, Moscow, ID 83844-3051, USA

[2] Department of Civil Engineering, University of Idaho, 875 Perimeter Dr. MS1022, Moscow, ID 83844-1022, USA

[3] Food Research Center, University of Idaho and Washington State University School of Food Science, Moscow, ID 83844-1052, USA

inoculate separate bioreactors wherein commercial quantities of PHA are produced (Dias et al. 2006; Serafim et al. 2008). When waste feedstocks are used, a fermentation step is incorporated upstream to convert the complex organic material therein (e.g., carbohydrates, proteins, and lipids) to volatile fatty acids (VFAs), which are the preferred precursors for PHA synthesis in these MMCs (Reis et al. 2003). This multi-stage PHA production approach has been successfully evaluated for multiple waste feedstocks, including paper mill effluent (Jiang et al. 2012), olive oil mill effluent (Dionisi et al. 2005), and molasses (Albuquerque et al. 2007). The overall success of this multi-stage PHA production approach is highly dependent on the enrichment of PHA-producing bacteria and their conditioning for high PHA storage.

The enrichment of MMCs for PHA production is most effectively accomplished through inducing and maintaining a particular metabolic response via the application of cyclic feast-famine conditions (referred to specifically as aerobic dynamic feeding, ADF) in a sequencing batch reactor (SBR) (Dias et al. 2006; Majone et al. 1996; Serafim et al. 2008). For a typical SBR cycle, substrate is added at the beginning of the cycle creating an excess of PHA precursors in solution (i.e., the feast phase). During the feast phase, PHA-producing bacteria simultaneously synthesize PHA (storage) and new biomass (growth), whereas bacteria lacking the PHA synthesis capacity simply grow (Dias et al. 2006; Reis et al. 2003; van Loosdrecht et al. 1997). For the remainder of the cycle following exogenous substrate depletion (i.e., the famine phase), bacteria with PHA mobilize their endogenous stores for carbon and energy to support continued growth and cellular maintenance, while bacteria lacking PHA stores decay (van Loosdrecht et al. 1997). Accordingly, PHA-producing bacteria exhibiting this feast-famine metabolic response can be enriched by combining short periods of exogenous substrate availability with long periods of exogenous substrate dearth (Johnson et al. 2009; Reis et al. 2003; van Loosdrecht et al. 1997).

The microbial community composition and associated physiology of MMCs in enrichment SBRs are recognized as being pivotal to PHA process performance. Considering microbial ecology, efforts to characterize the microbial community composition in SBRs have relied on the application of classical molecular methods including fluorescence in situ hybridization (FISH) coupled with PHA staining (Oehmen et al. 2014), clone library construction (Albuquerque et al. 2013), or denaturing gradient gel electrophoresis (Carvalho et al. 2013). In some investigations, links between microbial community composition and macro-level process performance were established (Albuquerque et al. 2013; Carvalho et al. 2013), with results that could be translated into engineering terms to improve PHA production (e.g., the development of segregated metabolic models accounting for substrate preferences by dominant populations (Albuquerque et al. 2013)). As such, resolving the microbial community composition of MMCs with respect to process performance may serve as an additional tool in guiding the determination of optimal bioreactor operating conditions. However, traditional molecular identification techniques may not be well suited for studies involving previously undefined microbial communities in SBRs cultivated on complex waste feedstocks, given the potential limitations in the depth of microbial community characterization. With advancements in high-throughput DNA sequencing technologies, enhanced resolution of microbial community composition is obtainable.

The microbial community functionality associated with a feast-famine response is dictated by the microbial community composition and physiological state. A conceptual basis for the microbial feast-famine response under ADF conditions has been established (as described above); however, little protein or enzymatic evidence is available to corroborate the observed feast-famine response in MMCs at a macro-level (i.e., bulk solution observations), as the direct characterization of microbial community functions has been limited. Nevertheless, to ultimately advance MMC PHA production using waste feedstocks, knowledge of microbial community functionality during an ADF SBR cycle and subsequent PHA production is required. In this regard, proteomics is a promising approach to characterize and elucidate microbial community functions (VerBerkmoes et al. 2009; Wilmes and Bond 2009). Indeed, the successful application of proteomics to obtain functional insight into microbial communities in engineered environments has been demonstrated in other studies, including activated sludge (Wilmes et al. 2008), membrane bioreactors (Kuhn et al. 2011; Zhou et al. 2015), and anaerobic digestion (Abram et al. 2011).

In the present study, genomic and proteomic tools were employed to investigate the microbial community composition and function in an enrichment SBR operated under ADF conditions using fermented dairy manure as the feedstock. 16S rRNA gene sequencing was performed using an Illumina MiSeq to characterize the microbial community composition of the MMC. Two-dimensional electrophoresis (2DE) was used to resolve MMC protein mixtures, allowing for the visualization and quantitative comparison of proteome dynamics during the SBR cycle as well as fed-batch PHA production assessments. Proteins of interest were excised from the 2DE gels and identified by nano-LC followed by QTOF mass spectrometry (LC-MS/MS). By integrating the microbial community composition and proteome-level data with bulk solution variables, a detailed examination of the MMC relative to PHA synthesis was made possible. To the authors' knowledge, this study is the first microbial community proteomic profiling of an MMC enriched under ADF conditions as part of a multi-stage PHA production system.

Materials and methods

Waste feedstock preparation

The fermented dairy manure liquor (FDML) feedstock for the PHA enrichment SBR was obtained from a 20-L dairy manure fermenter operated under conditions as previously described (Stowe et al. 2015). Briefly, manure was supplied from lactating Holstein cows at the University of Idaho Dairy, Moscow, ID. Effluent from the fermenter was poured through a stainless steel screen to remove large solids then centrifuged at 7650×*g* for 5 min to remove fine solids. The supernatant (i.e., the FDML) was then sterilized by autoclaving. To compensate for phosphate precipitation during autoclaving, equimolar KH_2PO_4 and K_2HPO_4 were added aseptically after cooling. The range of soluble VFA, ammonia, and phosphate concentrations in the final FDML feedstock are provided in Table 1.

Enrichment SBR operation

The enrichment SBR was operated under ADF conditions and with an operating volume of 1.8 L, a solid retention time (SRT) of 4 days, a hydraulic retention time (HRT) of 4 days, and a cycle length (CL) of 24 h. The cycle consisted of a fill phase (2 min), a react phase (1433 min), and a draw phase (5 min). Mixing was maintained throughout the cycle by a magnetic stir bar. House air was introduced into the SBR at a rate of approximately 1 L min^{-1} through a stainless steel diffuser to achieve aeration during the fill and react phases. FDML and autoclaved tap water were added to the reactor simultaneously during the fill phase, at a volumetric ratio of 40:60, respectively. The pumps and aeration were controlled by a programmable logic controller. The enrichment SBR was operated in a temperature-controlled room (20–26 °C) and the pH was monitored, but not controlled. When necessary (approximately once every 2 weeks), foaming was controlled with the addition of Antifoam A Concentrate (Sigma-Aldrich, St. Louis, MO, USA). The enrichment SBR was inoculated from a 20-L SBR (same SRT, HRT, and CL but fed non-sterilized FDML) that had been stably operated for 4 years (originally inoculated with an MMC from the Moscow, ID, wastewater treatment facility). After inoculation, the enrichment SBR was operated for approximately 2.5 months (equivalent to 18+ SRTs) to ensure the SBR had reached an equilibrated state. During that time, preliminary assessments of bulk solution variable changes (viz. VFA consumption, oxygen consumption, PHA accumulation, and biomass generation) were completed to confirm the enrichment SBR MMC was exhibiting a typical feast-famine response (i.e., for the feast phase, rapid VFA uptake, rapid decrease in dissolved oxygen (DO) concentration, and PHA synthesis; for the famine phase, steady increase in DO and depletion of PHA stores (Beun et al. 2002; Dionisi et al. 2004; Serafim et al. 2004)). Once the feast-famine response was stable, three independent sampling events (sampling #1, sampling #2, and sampling #3; sampling events were spaced two SRTs apart) spanning an operational cycle were completed.

Table 1 Characterization of fermented dairy manure liquor

Constituent[a]	Concentration[b]
HAc	43.2 mM ± 3.6
HPro	16.0 mM ±1.1
HBu	9.7 mM ±1.5
HiBu	1.6 mM ± 0.2
HVa	1.8 mM ± 0.2
HiVa	1.4 mM ± 0.5
HCa	0.6 mM ± 0.2
NH_3-N	24.2 mM ± 4.5
PO_4^{3-} –P	0.07 mM ± 0.03
COD	10,066 mg L^{-1} ± 1287

[a] *HAc* acetic acid, *HPro* propionic acid, *HBu* butyric acid, *HiBu* iso-butyric acid, *HVa* valeric acid, *HiVa* iso-valeric acid, and *HCa* caproic acid

[b] The concentration and standard deviation are indicated; $n = 9$ for all constituents

Fed-batch PHA production assessments

During each of the three sampling events, the enriched MMC from the SBR was also subjected to a fed-batch PHA production capacity assessment. Using the 450 mL of daily effluent from the enrichment SBR, the fed-batch assessments were conducted in a separate 1-L beaker under fully aerobic and completely mixed conditions using the same substrate (FDML feedstock and autoclaved tap water at a volumetric ratio of 40:60, respectively) that was used for the enrichment SBR cultivation. A total of three pulse additions of the substrate were applied at intervals determined by manually monitoring the DO concentration and adding the next feedstock pulse when the DO began to increase (Dias et al. 2006). The volume of each pulse addition was selected such that the VFA concentration in the fed-batch PHA production assessment after addition would approximate that in the enrichment SBR at the beginning of the feast phase (i.e., 112, 140, and 175 mL). The fed-batch assessments were carried out in the same temperature-controlled room (20–26 °C) and the pH was monitored, but not controlled.

Analytical procedures

DO, pH, and temperature were monitored using a Hach HQ40 meter with LDO101 and PHC101 probes (Hach, Loveland, CO). Total and volatile suspended solids (TSS and VSS, respectively) were determined in accordance with standard

methods (Eaton et al. 2005). Soluble VFAs (viz. acetic, propionic, butyric, valeric, caproic, iso-butyric, and iso-valeric acids) were quantified using a gas chromatograph equipped with a flame ionization detector as previously described (Coats et al. 2011). Soluble chemical oxygen demand (COD), phosphate (PO_4^{3-} –P), ammonia (NH_3-N), nitrite (NO_2^-N), and nitrate (NO_3^-N) concentrations were determined after sample filtration through a sterile 0.22-μm syringe filter (Millipore Corp., Billerica, MA) in accordance with standard methods (Eaton et al. 2005). The active biomass, X, was determined as the difference between the VSS and PHA (X = VSS − PHA) and was assumed to have the stoichiometric formula of $C_5H_7O_2N$ (Henze et al. 1995). Biomass PHA content was determined as methyl esters using gas chromatography-mass spectrometry (GC-MS) with minor modifications to procedures previously described (Dobroth et al. 2011). The maximum PHA content was calculated on a cell dry weight basis (i.e., mg PHA/mg TSS) and expressed as a percent. For consistency with other works in the field, VFA and PHA data is presented on a carbon millimole basis (i.e., Cmmol) (Roels 1983).

Microbial community analysis

Microbial genomic DNA was isolated from biomass samples using the PowerSoil DNA Isolation Kit (MOBIO, Carlsbad, CA) following the manufacturer's instructions. Genomic DNA yield and purity were quantified using a Synergy H1 Multi-Mode Reader (BioTek, Winooski, VT). Bacterial 16S rRNA gene fragments were amplified and sequenced following previously described methods (Dai et al. 2015; Liang et al. 2015) with minor modifications. Briefly, DNA amplicons were generated using two rounds of PCR: PCR1 amplified the targeted V1–V3 regions (*Escherichia coli* positions 27F-533R of the 16S rRNA gene) and PCR2 attached sequencing adapters and sample barcodes. PCR1 used the following primer sets listed according to position and direction:

27F-1:ACACTGACGACATGGTTCTACAGT
AGAGTTTGATCCTGGCTCAG;
27F-2:ACACTGACGACATGGTTCTACA
*C*GT**AGAGTTTGATCATGGCTCAG**;
27F-3:ACACTGACGACATGGTTCTACA
*AC*GT**AGAGTTTGATTCTGGCTCAG**;
27F-4:ACACTGACGACATGGTTCTACA
*TAC*GT**AGAGTTTGATTCTGGCTCAG**;
533R-1:TACGGTAGCAGAGACTTGGTCT
TTACCGCGGCTGCTGGCAC;
533R-2:TACGGTAGCAGAGACTTGGTCT
*G***TTACCGCGGCTGCTGGCAC;**
533R-3:TACGGTAGCAGAGACTTGGTCT
*TG***TTACCGCGGCTGCTGGCAC;**
533R-4:TACGGTAGCAGAGACTTGGTCT
*ATG***TTACCGCGGCTGCTGGCAC.**

The underlined sequences denote universal tag sequences CS1 (ACACTGACGACATGGTTCTACA; tag on the forward primer) and CS2 (TACGGTAGCAGAGAC TTGGTCT; tag on the reverse primer), the bold sequences denote the universal 16S rRNA primers 27F and 533R, and the italicized bases denote the added bases to the template-specific primers in order to introduce variability of base calls during Illumina sequencing. For PCR2, the adapter primers included the Illumina-specific sequences P7 and P5 for dual indexing:

P7-CS2: CAAGCAGAAGACGGCATACGAGAT*NNN NNNNN*TACGGTAGCAGAGACTTGGTCT;
P5-CS1: AATGATACGGCGACCACCGAGATCTAC AC*NNNNNNNN*ACACTGACGACATGGTTCTACA, where the unique sequence barcodes were denoted by the eight italicized N's and the underlined sequences denote the universal sequences CS1 and CS2.

Amplicon concentrations were determined using the PicoGreen assay (Molecular Probes Inc., USA) and a fluorometer (SpectraMax Gemini XPS 96-well plate reader, Molecular Devices, Sunnyvale, CA). The amplicons were pooled into a single tube in approximately equal amounts (~100 ng). The amplicon pool was then cleaned to remove short, undesirable fragments following the procedures previously reported (Dai et al. 2015; Liang et al. 2015). Finally, sequences were obtained using an Illumina MiSeq paired-end 300 bp protocol (Illumina, Inc., San Diego, CA).

For sequence analysis and taxonomic classification, raw DNA sequence reads from the Illumina MiSeq were demultiplexed and subsequently processed to identify and assign reads by both expected barcode and primer sequences using the python application *dbcAmplicons* (https://github.com/msettles/dbcAmplicons). Briefly, barcodes were allowed to have at most one mismatch and primers were allowed to have at most four mismatches (as long as the final four bases of the primer matched the target sequence perfectly). Reads were then trimmed of their primer sequence and joined into a single amplicon sequence using the application *FLASH* (Magoč and Salzberg 2011). Finally, the Ribosomal Database Project (RDP) Bayesian classifier was used to assign sequences to phylotypes (Wang et al. 2007); reads were assigned to the first RDP taxonomic level with a bootstrap score ≥50. The relative abundance of individual phylotypes in each sampling event was determined as the percentage of the corresponding sequence reads among all sequence reads. The sequencing data is available through the National Center for Biotechnology Information Short Reads Archive (http://www.ncbi.nlm.nih.gov/sra) identifier

SRA307139. Microbial community data analysis was performed using *R* v3.2.2 software (http://www.r-project.org/) using the *vegan* package.

Protein extraction, purification, and 2DE

Samples for proteome profiling during the SBR cycle were collected at 1, 4.5, 11.5, 17.5, and 23.5 h from the start of the cycle (Fig. 1). The 1-h sample represented activity within the feast phase of the SBR cycle, and the remaining samples represented activity within the famine phase of the SBR cycle. For fed-batch proteomic profiling, a sample was collected approximately 1 h after the third feedstock addition. The three sampling events therefore constitute three biological replicates for each of the time points.

Bacterial protein extraction from the biomass, purification, and 2DE were performed following methods previously described (Hanson et al. 2016). Briefly, bacterial cells were first separated from MMC biomass samples by Accudenz gradient centrifugation. Bacterial cell disruption and sequential protein extraction were performed by sonication and bead mill beating. Protein concentrations were determined using the RCDC Protein Assay (Bio-Rad, Hercules, CA) following the manufacturer's instructions using bovine serum albumin as the protein standard. Protein purification for 2DE was performed using the ReadyPrep 2DE Cleanup Kit (Bio-Rad), and 400 μg of purified protein was loaded onto 7 cm immobilized pH gradient (IPG) strips with a pH range of 4–7 (Bio-Rad), which were passively rehydrated for 16 h at 22 °C. IPG strips were focused in a PROTEAN isoelectric focusing (IEF) cell (Bio-Rad) at 250 V for 15 min, followed by linear ramping to 4000 V in 2.5 h, after which 4000 V was held for approximately 3.25 h (total of 13,000 Vh). Immediately following IEF, IPG strips were equilibrated and subjected to SDS PAGE for protein separation by molecular weight. After SDS PAGE, gels were washed twice in double-deionized H_2O for 5 min, fixed in ethanol/acetic acid/water (40:10:50, *v*/*v*) for 30 min, stained with Coomassie Brilliant Blue G-250 (Bio-Rad) for 20 h, and de-stained with double-deionized H_2O for several hours prior to imaging.

2DE gel image acquisition and statistical analysis

2DE gels were scanned using an Odyssey Imaging System (Li-COR Biosciences, Lincoln, NE) with the following settings: resolution, 42 μm; quality, medium; channel, 700 nm; and focus offset, 0.5. These settings generated 16-bit, 600 DPI images which were saved as TIFF files. Gel images were analyzed using *REDFIN 3 Solo* Software (Ludesi, Malmö, Sweden, http://www.ludesi.com). After image quality control checks were passed, anchor points were manually set using features shared by all gel images. The software was used to warp each of the gel images to a reference based on the shared anchor points, creating a composite image. Protein spot intensities were calculated with background correction and normalized to correct for systematic differences in gel intensity. Replicate gel variability was assessed by constructing a correlation matrix based on the spot intensities using Pearson's product moment correlation coefficient (Wilmes and Bond 2004). The feast phase (1 h) was compared to the individual time points of the famine phase (4.5, 11.5, 17.5, and 23.5 h), and protein samples from the fed-batch PHA production assessments were compared to protein samples from the enrichment SBR; ANOVA was applied to determine protein spots exhibiting statistically significant differential abundance (taken to be at least a twofold change in protein spot intensity with an accompanying p value <0.05).

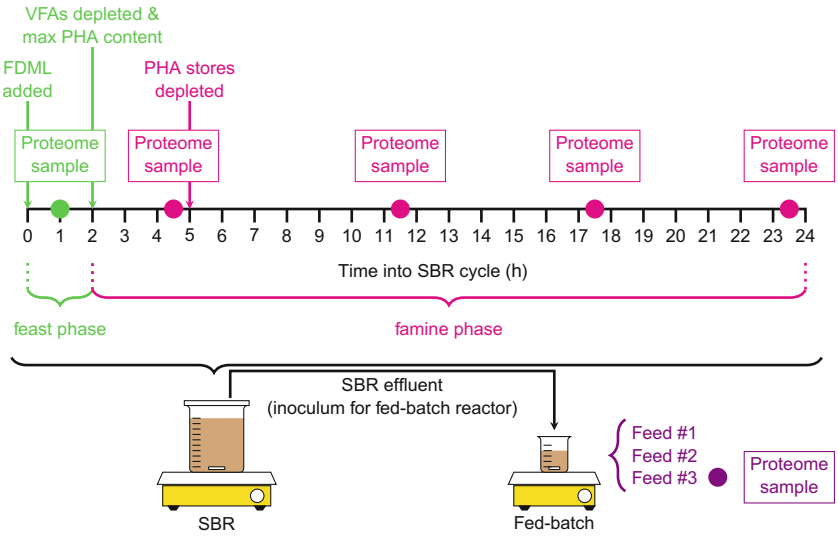

Fig. 1 Proteomic sampling scheme for enrichment SBR and fed-batch PHA production samples. Approximate times are shown for VFA depletion, maximum PHA content reached, and PHA depletion. The times at which proteome samples were taken during the SBR cycle are indicated by the *solid circles*. The proteome samples for the fed-batch PHA production assessments were taken approximately 1 h after the third feedstock addition

In-gel trypsin digestion, LC-MS/MS, and proteomic data analysis

Protein spots of interest were manually picked from gels using a 1.5-mm OneTouch Plus Spotpicker (The Gel Company, San Francisco, CA) with disposable tips and transferred to microfuge tubes. In-gel trypsin digestion was performed with minor modifications following previously described procedures (Shevchenko et al. 2006). Gel pieces were de-stained overnight with light shaking in approximately 500 μL 50 % acetonitrile (*v*/*v* in H_2O) and 25 mM ammonium bicarbonate. The extract was discarded and 50 μL 100 % acetonitrile was added to completely dehydrate the gel pieces. After the gel pieces became opaque, they were washed with 25 mM ammonium bicarbonate and dehydrated again by adding 50 μL acetonitrile; the acetonitrile was then evaporated. The dried gel pieces were rehydrated in an excess volume of 12.5 ng μL^{-1} sequencing grade trypsin (Promega, Madison, WI) solution for 1.5 h at 4 °C. Excess trypsin solution was removed and a small volume (~25 μL) of 25 mM ammonium bicarbonate was added to cover the gel pieces to ensure no evaporation occurred for the duration of the enzymatic digestion. Gel pieces were then incubated for 16 h at 37 °C. The water extracts were retained in LoBind 0.5 mL microcentrifuge tubes (Eppendorf, Hauppauge, NY), after which peptides were eluted from the gel pieces using 50 % acetonitrile in water containing 0.1 % formic acid with light vortexing for 15 min. Samples were centrifuged briefly and the extracts were retained. The elution step was repeated and extracts were concentrated using a SpeedVac until approximately 10 μL remained. Prior to analysis by liquid chromatography-tandem mass spectrometry (LC-MS/MS), approximately 10 μL of 5 % acetonitrile with 0.1 % formic acid was added to the sample, which was then clarified by centrifugation at 16,000×*g* for 10 min.

LC-MS/MS proteomic analysis was similar to reported methods (Bansal et al. 2009; Checinska et al. 2012) with modifications. Peptides were separated using reverse-phase LC on a nano-ACQUITY Ultra Performance Liquid Chromatograph (Waters Corporation, Milford, MA) prior to analysis using a QTOF Premier tandem mass spectrometry system equipped with a nano-electrospray ionization (ESI) source. A 2-μL sample was first loaded onto a Symmetry C18 trap column (0.18 mm × 20 mm, Waters Corp. P/N 186002841) before separation using a BEH 130 C18 analytical column (0.100 μm × 100 mm; Waters Corp. P/N 186003546). Two solvents were used: A, 0.1 % formic acid in water and B, 0.1 % formic acid in acetonitrile. Peptides were trapped using 100 % solvent A for 3 min with a flow rate of 8 μL min^{-1}. Separation was performed at 35 °C at a flow rate of 0.4 μL min^{-1} with the following conditions: (i) isocratic, 1 min, 95 % solvent A and 5 % solvent B; (ii) gradient, 10 min, solvent A concentration decreased from 95 to 85 % and solvent B concentration increased from 5 to 50 %; (iii) gradient, 10 min, solvent A concentration decreased to 73 % and solvent B concentration increased to 27 %; (iv) gradient, 10 min, solvent A concentration decreased from 59 % and solvent B concentration increased to 41 %; (v) gradient, 10 min, solvent A concentration decreased to 43 % and solvent B concentration increased to 57 %; (vi) gradient, 14 min, solvent A concentration decreased to 10 % and solvent B concentration increased to 90 %; (vii) isocratic, 5 min, 10 % solvent A and 90 % solvent B; and (viii) gradient, 10 min, solvent A concentration increased to 95 % and solvent B concentration decreased to 5 %. The nano-ESI source was operated with the following settings: capillary voltage, 3.65 kV; cone voltage, 42 V; source temperature, 110 °C; nebulizing gas pressure, 0.17 bar; collision energy, 3.0 V; detector voltage, 2150 V. The data acquisition was performed using MS survey mode with the following parameters: mass range, 300 to 2000 Da; scan time, 1 s; and interscan delay, 0.05 s. The threshold of MS/MS acquisition was 15 counts per second with the following settings: mass range, 50 to 2000 Da; 3 ions selected from a single MS survey scan; scan time, 2 s; and interscan delay, 0.05 s. [Glu1]-fibrinopeptide B (Sigma-Aldrich, St. Louis, MO) was used for dynamic calibration (lockmass) with a 30-s frequency.

The raw data files from the peptide sequencing were converted to peak list files by *ProteinLynx Global Server* 2.3 software (Waters Corporation) using the following parameters: (i) smooth channels, 4; number of smooths, 2; smooth mode, Savitzy-Golay; (ii) peak height to calculate the centroid spectra, 80 %; (iii) baseline subtraction, none allowed; and (iv) peptide tolerance, 100 ppm. Mascot (v2.5, Matrix Science, London, UK) was used for MS/MS ions matching and protein identification. The peak list files were searched against the NCBInr database (October 2015; 73,055,898 protein sequences) with no species restriction and the following search parameters: (i) specific enzyme, trypsin; (ii) peptide window tolerance, ±0.4 Da; (iii) fragment mass tolerance, ±0.4 Da; (iv) missed cleavage sites, 1; and (v) variable modifications, carbamidomethyl C, deamidated NQ, and oxidized M. The decoy option was included for each search to determine the false discovery rate. For protein identification, protein hits with at least two peptide matches and individual protein scores above the significance score calculated by Mascot ($p < 0.05$; the individual ion score is $-10 \times \log(p)$, where p is the probability that the observed match is the random match) were accepted. In instances when more than one protein was assigned from a single protein spot (a well-established occurrence for 2DE (Thiede et al. 2013)), the highest scoring protein was accepted and the other proteins meeting the search criteria were recorded. When a hypothetical protein was the highest scoring Mascot result, the corresponding protein accession number was searched using Blastp for homology-based protein identification; the protein match with the highest

percent similarity based on the number of identical amino acids to a known bacterial protein was considered for identification. The mass spectrometry proteomics data have been deposited to the ProteomeXchange Consortium (http://proteomecentral.proteomexchange.org) via the PRIDE partner repository (Vizcaino et al. 2013) with the dataset identifier PXD003126 (http://dx.doi.org/10.6019/PXD003126).

Results

Enrichment SBR and fed-batch PHA production performance

To induce a feast-famine response in the MMC, ADF conditions were applied to an enrichment SBR using fermented dairy manure as the feedstock. Shortly after startup (9 days), the DO began to exhibit the characteristic feast-famine profile (Beun et al. 2002; Dionisi et al. 2004; Serafim et al. 2004). During the 2.5-month SBR stabilization period, VFA depletion from solution typically occurred within 2–3 h and the maximum PHA content ranged from 4–14 % (wt. basis; data not shown). Concerning the composition of the FDML during sampling (summarized in Table 1), seven different VFAs were consistently identified in the FDML, with acetate and propionate dominating at 50 and 23 % (wt. basis), respectively, of the total VFA content. In total, the VFAs accounted for approximately 70 % (wt. basis) of the COD. The ammonia and phosphate concentrations were 24.2 mM ± 4.5 and 0.07 mM ± 0.03, respectively.

Representative profiles of select bulk solution parameters are depicted in Fig. 2 (all sampling data is provided in Figs. S1–S6). During the feast phase, VFA consumption was zero order (Fig. 2a), with acetate being consumed at the highest rate (average specific uptake rate for all three sampling events was 0.040 ± 0.010 Cmmol HAc Cmmol X^{-1} h^{-1}) followed by propionate (average specific uptake rate for all three sampling events was 0.030 ± 0.007 Cmmol HPro Cmmol X^{-1} h^{-1}); the average total specific VFA uptake rate was 0.091 ± 0.024 Cmmol VFA Cmmol X^{-1} h^{-1}. All measured VFAs were depleted within 2.5 h (which corresponded with the apparent depletion of readily biodegradable COD; Fig. S1), at which point the DO exhibited the first notable increase (Fig. 2c). Coinciding with VFA depletion, the maximum PHA content was observed (8–16 % wt. basis; shown in Fig. 2b as Cmmol PHA L^{-1}); the PHA yield ranged from 0.36 to 0.88 Cmmol PHA Cmmol VFA^{-1} for the three sampling events. The average TSS during the feast phase for the three sampling events was 2758 ± 377 mg L^{-1}. A copolymer of HB and HV was consistently synthesized, with average HV fractions throughout the cycle of 0.70 ± 0.07, 0.60 ± 0.10, and 0.70 ± 0.05 mol HV mol PHA^{-1} for sampling #1, sampling #2, and sampling #3,

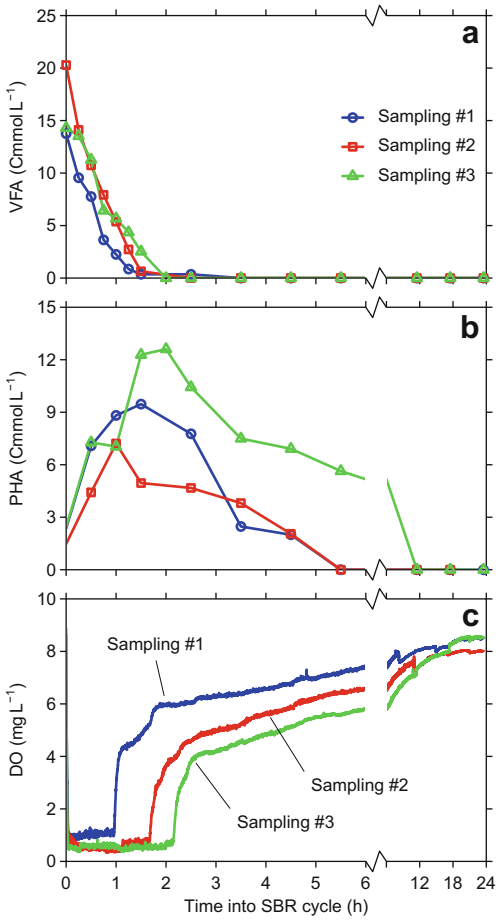

Fig. 2 Concentration profiles of select bulk solution variables during an SBR cycle. **a** Total VFAs, **b** total PHA, and **c** dissolved oxygen. Note the break and scale change in the abscissa at 6 h

respectively. Ammonia, nitrite, and nitrate consumption was also observed during the feast phase (Fig. S2), and the VSS concentrations remained approximately constant (Fig. S3). The pH decreased slightly with substrate addition to approximately 8.6, before increasing to approximately 9.1, and the temperature increased slightly (Figs. S4–S5).

The famine phase commenced with the depletion of VFAs and the first notable increase in DO concentration. Within the famine phase, PHA stores were depleted approximately 4.5–10 h after VFA exhaustion. The depletion of PHA corresponded to the next notable increase in DO concentration (Fig. 2c). Near-complete ammonia removal was realized by the end of the SBR cycle (Fig. S2; final concentrations ranged from 0.017 to 0.28 mM). Both nitrite and nitrate gradually increased during the famine phase (Fig. S2; final concentrations ranged from 1.04 to 4.36 mM and 0.41 to 1.01 mM for nitrite and nitrate, respectively). Continuing from the end of the feast phase, COD and VSS remained approximately constant (Figs. S1 and S3, respectively; final concentrations ranged from 875 to 1242 mg L^{-1} for COD and 1267 to 2700 mg L^{-1} for VSS). The average TSS during the famine

phase for the three sampling events was 2653 ± 571 mg L^{-1}. The pH decreased to approximately 8.5, increasing to approximately 8.8, whereas the temperature slightly decreased (Figs. S4–S5).

For each of the enrichment SBR sampling events, a parallel fed-batch PHA production assessment was completed to evaluate the PHA production capacity of the enriched MMC. The maximum PHA content measured during the fed-batch assessments ranged from 22 to 40 % (wt. basis; shown as Cmmol PHA L^{-1} in Fig. S6); the highest PHA content was achieved on sampling #1 (40 %). The PHA yield ranged from 0.55 to 1.14 Cmmol PHA Cmmol VFA^{-1} and was determined at the time of maximum PHA content as the total amount of PHA produced divided by the total amount of VFAs consumed from the start of the fed-batch assessment. Similar to the enrichment SBR, the copolymer PHBV was produced with average HV fractions throughout the production assessment of 0.75 ± 0.03, 0.67 ± 0.06, and 0.59 ± 0.09 mol HV mol PHA^{-1} for sampling #1, sampling #2, and sampling #3, respectively.

Microbial community analysis

To characterize the microbial composition of the MMC in the enrichment SBR, amplicons of the V1–V3 region of the 16S rRNA gene were sequenced and assigned to phylotypes. A total of 70,004 high-quality sequences from the three sampling events (average of 23,334 reads per sample) were obtained; sequencing coverage depth was considered sufficient for each sample based on rarefaction analysis (Fig. S7). An overview of the microbial community composition (from sampling #1) is shown in Fig. 3a (the other sampling events are displayed in Figs. S9–S10), and the best classification of phylotypes from all sampling events is shown in Fig. 3b. A total of 24 bacterial phyla were identified in the MMC (Table S1). *Proteobacteria* was the most abundant phylum (73–75 %) for each sampling event, followed by *Bacteroidetes* (15–18 %). Less abundant phyla included *Verrucomicrobia* (0.6–3 %) and *Planctomycetes* (0.5–3 %), *Actinobacteria* (1.2–1.8 %), and *Chloroflexi* (0.7–1 %). Eighteen minor (each <1 % of the total abundance) bacterial phyla accounted for the approximately 1.5 % remaining of the total abundance at the phylum level. At the class level (Table S2), within *Proteobacteria*, *Alphaproteobacteria* was the most abundant (43–68 %), followed by *Betaproteobacteria* (5–21 %), *Deltaroteobacteria* (1.5–9 %), and *Gammaproteobacteria* (1–7 %). Within *Bacterioidetes*, *Sphingobacteriia* was the most abundant class (10–11 %), followed by *Flavobacteriia* (3–6 %). Forty-one minor (each <1 % of the total abundance) classes comprised the approximately remaining 3 % of the total abundance at the class level.

The number of phylotypes classified by the RDP was 217, 298, and 342 for sampling #1, sampling #2, and sampling #3, respectively. The Shannon index (selected for its value as a general diversity measure considering both richness and evenness (Hill et al. 2003)) values were 2.20, 3.31, and 3.00 for sampling #1, sampling #2, and sampling #3, respectively. As shown in Fig. 3b, *Meganema* was the most abundant genus in all samples (31–61 %). For sampling #1, other genera included *Terrimonas* (4.6 %) and *Thauera* (2.2 %); minor phylotypes (each <1 % of the total abundance) comprised 15 % of the total abundance. For sampling #2, other genera included *Thauera* (8 %), *Nannocystis* (6 %), *Flavitalea* (6 %), *Hyphomonas* (2.7 %), and *Terrimonas* (2.6 %); minor phylotypes comprised 22 % of the total abundance. For sampling #3, other genera included *Thauera* (12 %), a member of *Flavobacteriales* (4.6 %), *Terrimonas* (3 %), *Flavitalea* (2.7 %), and *Nannocystis* (2 %); minor phylotypes comprised 18 % of the total abundance.

2DE analysis and proteomic profiling

To visualize and quantify changes in protein abundance under ADF conditions using FDML as a feedstock, 2DE was used to resolve protein mixtures from the MMC in the enrichment SBR at five time points during an operational cycle, as well as a single time point during the accompanying fed-batch PHA production assessments. The average protein concentration in whole cell lysates ranged from 9.6 to 15.2 mg mL^{-1} (Fig. S11). An example set of 2DE gels is shown in Fig. 4; all other gels are shown in Figs. S12–S13. The resulting 2DE spot patterns for replicate gels exhibited a strong correlation with coefficients ranging from 0.71 to 0.95 (Table S3). As shown in Fig. 4, protein spots were well resolved and exhibited a range of apparent molecular weights (~10–190 kDa) and isoelectric points (within pH 4–7). In total, 712 protein spots were detected on the composite image of all 18 gels created using the *REDFIN 3 Solo* software. Lastly, horizontal streaking and diffuse background interference on the gels were minimal.

Protein spots that displayed high abundance across all gels and those that exhibited large, statistically significant abundance changes between the feast and famine phases or between the SBR samples and fed-batch samples were given priority in selection for LC-MS/MS proteomic analysis. In total, 90 protein spots were selected for LC-MS/MS, 83 of which generated peptide spectra that could be searched using Mascot. Overall, 157 proteins met the search criteria for an acceptable protein match from the 83 successfully analyzed protein spots (some spots had more than one identified protein). Of those, 74 protein identifications were accepted in relation to the prioritized protein spots (Tables 2, 3, 4, and 5; a complete list with protein identification information is provided in Table S5). *Meganema perideroedes* was the most common microorganism for protein assignments with 149 of the 157 proteins assigned accordingly. As 69 of the protein assignments were hypothetical proteins, Blastp was used for homology-based identification (Table S6);

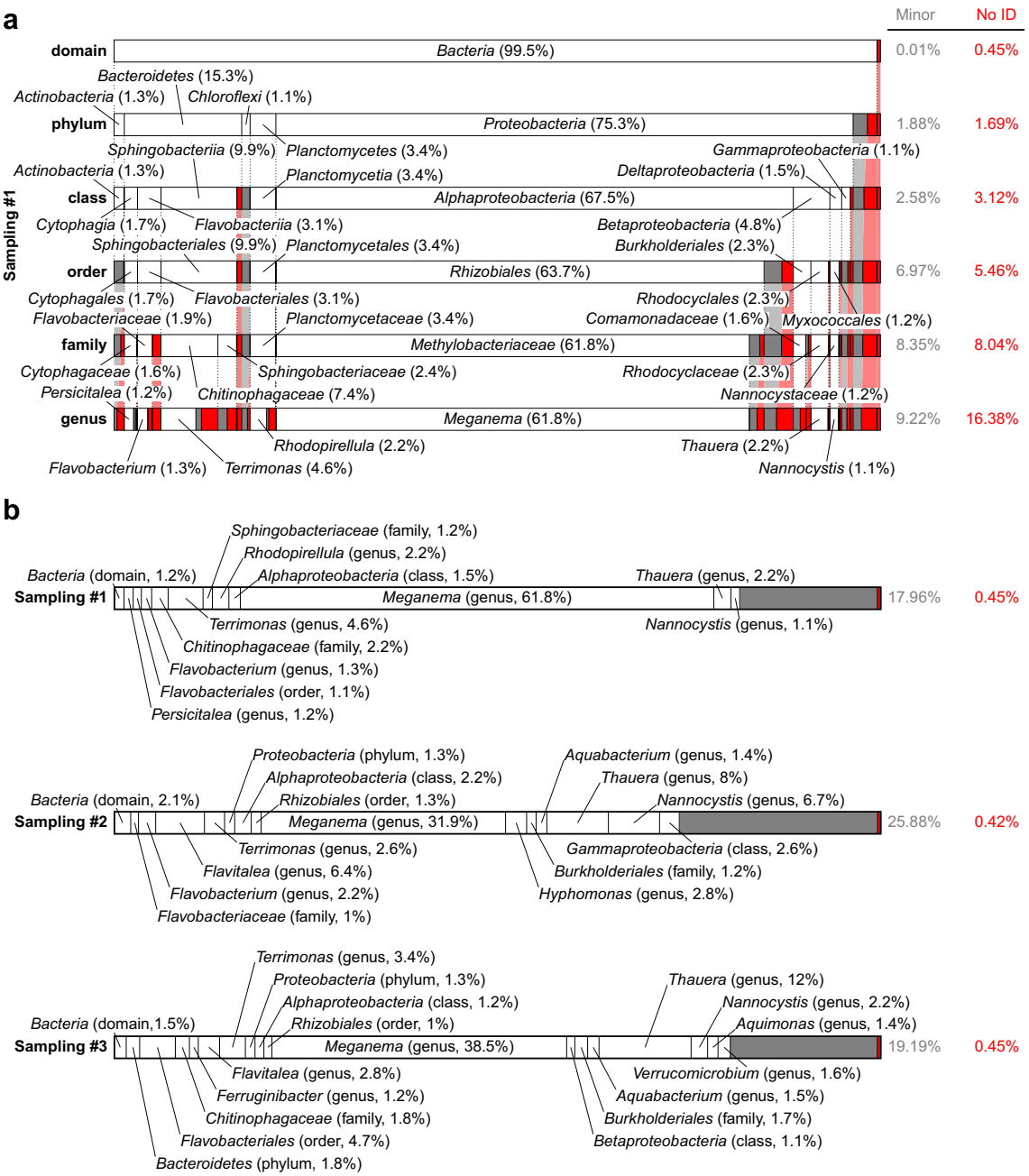

Fig. 3 Relative abundance and taxonomic classification of the 16S rRNA gene sequencing results using the RDP. The classified phylotypes are depicted in terms of the taxonomic hierarchy (**a**) and as the best classification (**b**). In both **a** and **b**, phylotypes which were not identified by the RDP or those whose identification at a specific taxonomic level was not statistically significant were aggregated, denoted "No ID," and depicted in *red*. Identified phylotypes with less than 1 % of the total relative abundance were aggregated, denoted "*Minor*," and depicted in *gray*. Phylotypes with at least 1 % relative abundance are labeled

49 of the hypothetical proteins were matched with >50 % amino acid identity to known bacterial proteins, and the 20 remaining hypothetical proteins were matched with 31–49 % amino acid identity. Generally, the observed molecular weight and isoelectric points of the selected protein spots were in agreement with calculated values.

As stated previously, protein spots displaying high abundance on gels were prioritized for LC-MS/MS analysis. Five highly abundant protein spots, each observed with an individual average normalized volume >1 % of the total spot volume on all 18 gels, were first selected for identification. In order of average abundance of each protein spot on all gels, these proteins were identified as a porin, superoxide dismutase, bacterioferritin, and two ABC transport proteins (Table 2).

For the feast phase, 28, 30, 44, and 33 proteins exhibited statistically significant abundance increases relative to the

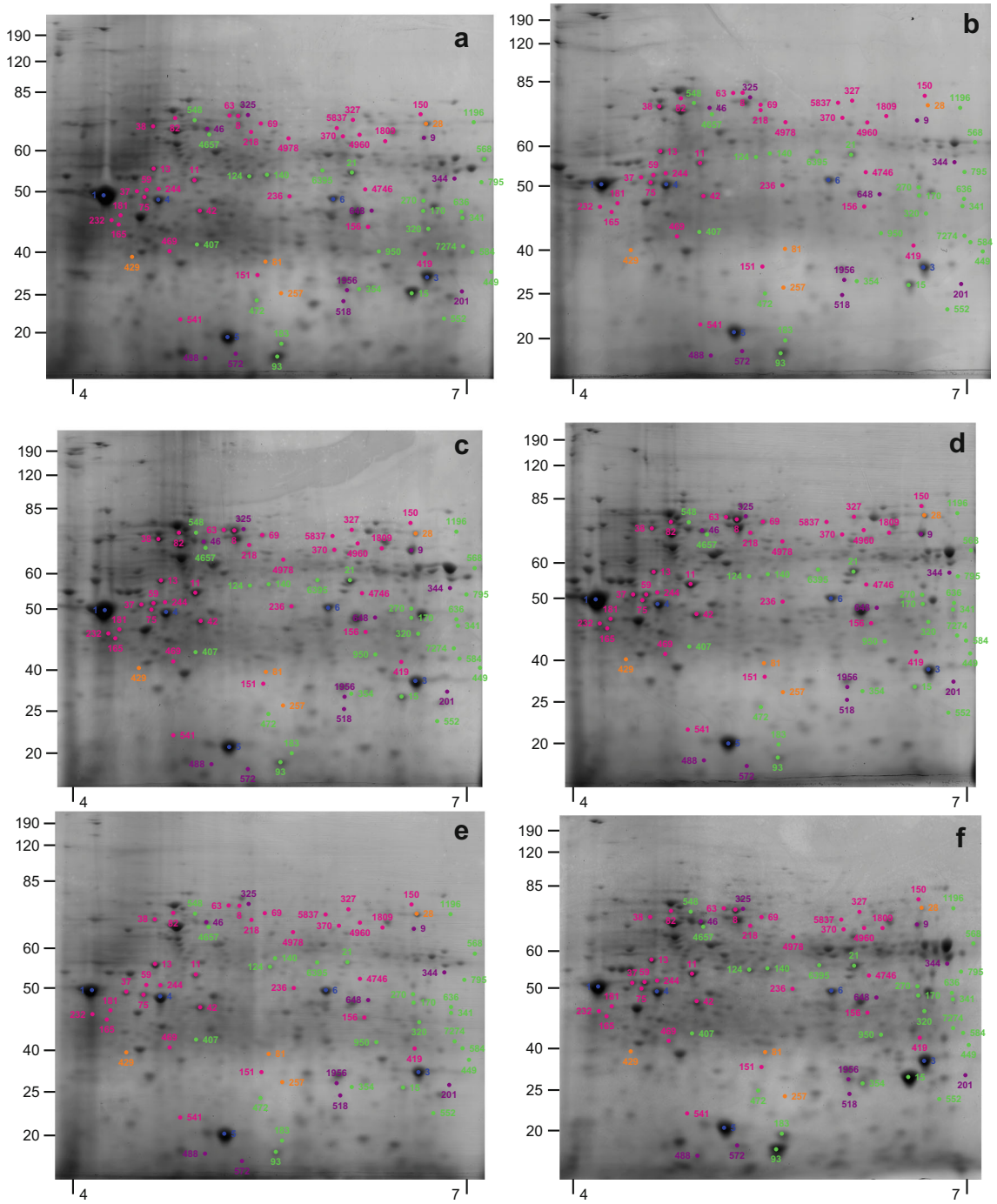

Fig. 4 Representative colloidal Coomassie-stained 2DE gel images for the SBR and fed-batch PHA production MMC proteins. Gel images are from sampling #3; **a**–**e** represent the samples taken throughout the SBR cycle; **f** represents the sample taken during the fed-batch PHA production assessment (as depicted in Fig. 1). The contrast for the 2DE gel images was uniformly adjusted across all images. The molecular weight markers (kDa) and pH ranges are depicted on each 2DE gel image. The *colored numbers* highlight protein spots that were identified with the most abundant protein spots in *blue*, proteins exhibiting increased abundance during the feast phase in *green*, proteins exhibiting increased abundance during the famine phase in *magenta*, proteins exhibiting increased abundance in the fed-batch in *violet*, and proteins exhibiting increased abundance in the SBR in *orange* (respective proteins are listed in Tables 2, 3, 4, and 5 and the abundances are in Figs. S15–S88)

famine phase samples at 4.5, 11.5, 17.5, and 23.5, respectively. In total, 25 protein spots from the feast phase were identified (Table 3). Of particular interest, PHA synthesis-related proteins, namely acetyl-CoA acetyltransferase and a phasin protein, were identified. Other identified proteins exhibiting increased abundance during the feast phase included three associated with protein synthesis, two TCA cycle enzymes, two uncharacterized membrane proteins, aldehyde dehydrogenase,

Table 2 Identification and functional characterization of the most abundant proteins observed on all 2DE gels

Spot	Protein name[a]	Accession	Mascot score	Matched peptides	MW[b]	pI[c]	General function
1	Porin*	WP_018631314	227	4	36,221	4.53	Nutrient transport
3	Superoxide dismutase*	WP_018632695	209	4	21,878	5.89	Reactive oxygen species destruction
5	Bacterioferritin	WP_026310284	227	4	18,528	4.95	Iron homeostasis
4	Amino acid ABC transporter substrate-binding protein*	WP_018632268	722	8	37,781	4.89	Nutrient transport
6	ABC transporter substrate-binding protein*	WP_018631899	614	9	39,576	6.36	Nutrient transport

[a] An * indicates homology-based identification of a hypothetical protein using Blastp (see Table S6 for related information)

[b] The calculated molecular weight of the identified protein

[c] The calculated isoelectric point of the identified protein

methylmalonate-semialdehyde dehydrogenase, malyl-CoA lyase, 2,5-didehydrogluconate reductase, and translocation protein TolB. Evaluating functionally related feast phase proteins over the SBR cycle (Figs. S20–S39), phasin proteins generally decreased in abundance until the end of the cycle (23.5 h). Both TCA cycle enzymes appeared to decrease at 4.5 h and then remain approximately constant until the end of the cycle. Translation proteins (elongation factor Tu and 50S ribosomal protein L6) appeared to decrease at 4.5 h and then remain approximately constant for the rest of the cycle. Other PHA synthesis-related proteins (i.e., NADPH-dependent acetoacetyl-CoA reductase and PHA synthase) were detected (Table S5), but the abundance and temporal characteristics could not be specifically determined, as the peptides originated from combined samples of multiple protein spots.

For the famine phase, 24, 19, 25, and 13 proteins exhibited statistically significant increased abundance at 4.5, 11.5, 17.5, and 23.5 h, respectively, compared to the feast phase (1 h). In total, 30 protein spots from the famine phase were identified (Table 4). Identified proteins included 11 ABC transport proteins, four enzymes associated with acyl-CoA metabolism, two subunits of the ATP synthase complex, quinohemoprotein amine dehydrogenase, glycerol kinase, fumarate hydratase, quinone oxidoreductase, molecular chaperone GroEL, TelA, 2′3′-cyclic-nucleotide 2′phosphodiesterase, Fis family transcriptional regulator, elongation factor Tu, and an uncharacterized membrane protein. Evaluating the abundance of functionally related famine phase proteins over the SBR cycle (Figs. S45–S72), most of the ABC transport proteins appeared to steadily increase as the famine progressed, with the highest abundance at 23.5 h. Other protein groups (e.g., proteins involved in acyl-CoA metabolism, housekeeping functions, and energy production) did not appear to exhibit a common trend.

Finally, comparing the fed-batch to the SBR samples, 19 protein spots exhibited statistically significant increases in abundance in the fed-batch compared to the SBR; of these proteins spots, 10 were selected for LC-MS/MS analysis (Table 5). Identified proteins included a phasin, two subunits of ATP synthase, methylmalonate-semialdehyde dehydrogenase, malate dehydrogenase, an ABC transport protein, and molecular chaperone GroEL. Inverting the comparison (i.e., comparing the SBR samples to the fed-batch PHA production samples), six proteins were in higher abundance in all of the SBR samples compared to the fed-batch PHA production samples. Of those, four were selected for LC-MS/MS analysis and identified (Table 5) as dihydrolipoamide dehydrogenase, adenylate kinase, an amino acid transporter, and a transcription/antitermination factor.

Discussion

Enrichment SBR and fed-batch process performance

The objective of this research was to develop an enhanced understanding of MMC structure function associated with a feast-famine PHA synthesis response when cultivated on fermented dairy manure under ADF conditions. The establishment of a feast-famine metabolic response using this feedstock and the applied ADF conditions was validated through the observed bulk solution changes (e.g., VFA uptake, DO profile, PHA synthesis, and mobilization). Bulk solution MMC-influenced parameters in this study, including VFA consumption rates, maximum PHA content, and PHA production yields in the enrichment SBR, were in line with other studies using fermented waste feedstocks (Morgan-Sagastume et al. 2010; Oehmen et al. 2014). Consistent with VFA uptake, COD was consumed during the feast phase; COD remained approximately constant during the famine phase, suggesting the residual COD was either recalcitrant or too slowly biodegradable to be appreciably consumed within the SBR cycle. Thus, even though non-VFA carbon sources were not monitored, the results suggested that the VFAs in the FDML were the primary substrates driving PHA synthesis.

Table 3 Identification and functional characterization of protein spots exhibiting at least a twofold change increase in abundance during the feast phase relative to the famine phase

Spot	Fold change	Time (h)[a]	Protein name[b,c]	Accession	Mascot score	Matched peptides	MW[d]	pI[e]	General function
341	3.3	23.5	Isocitrate dehydrogenase	WP_018631946	237	4	44,956	6.04	Energy generation and conversion
407	3.8	23.5	Aldehyde dehydrogenase	WP_018633284	302	4	55,302	6.14	Energy generation and conversion
584	8.5	23.5	Malate dehydrogenase	WP_018631935	82	2	33,324	5.49	Energy generation and conversion
636	3.0	17.5	Isocitrate dehydrogenase[§]	WP_003813356	145	2	45,249	5.24	Energy generation and conversion
950	5.3	11.5	Methylmalonate-semialdehyde dehydrogenase*	WP_018632449	142	2	54,008	5.94	Energy generation and conversion
1196	3.9	17.5	Aldehyde dehydrogenase	WP_018633284	433	7	55,302	6.14	Energy generation and conversion
7274	3.2	4.5	Malate dehydrogenase[§]	WP_020951282	189	3	33,433	5.34	Energy generation and conversion
21	3.1	23.5	Acetyl-CoA acetyltransferase	WP_018631634	711	9	40,685	5.97	PHA synthesis
15	6.7	23.5	Phasin*	WP_018634051	493	7	18,623	5.80	PHA synthesis
93	4.2	17.5	Phasin*	WP_018634051	468	7	18,623	5.80	PHA synthesis
183	5.4	23.5	Phasin*	WP_018634051	348	6	18,623	5.80	PHA synthesis
354	6.3	23.5	Phasin*	WP_018634051	520	7	18,623	5.80	PHA synthesis
472	4.5	23.5	Phasin*	WP_018634051	213	4	18,623	5.80	PHA synthesis
568	4.1	23.5	Acetyl-CoA acetyltransferase	WP_018631634	545	8	40,685	5.97	PHA synthesis
124	4.3	17.5	Elongation factor Tu	WP_018631570	627	11	43,422	5.42	Translation
140	2.8	4.5	Elongation factor Tu	WP_018631570	369	7	43,422	5.42	Translation
449	17.6	23.5	50S ribosomal protein L6	WP_018631584	138	2	21,182	9.21	Translation
6395	3.5	11.5	Elongation factor Tu	WP_018631570	286	5	43,422	5.42	Translation
548	3.3	17.5	Molecular chaperone GroEL	WP_018633070	184	4	57,962	5.05	Posttranslation protein modification
4657	3.4	23.5	Molecular chaperone GroEL	WP_018633070	214	5	57,962	5.05	Posttranslation protein modification
270	2.2	17.5	Malyl-CoA lyase*	WP_018632386	137	3	34,755	5.82	Carboyhydrate transport and metabolism
170	3.2	23.5	Translocation protein TolB	WP_026310348	182	4	47,660	9.40	Intracellular trafficking
320	4.1	4.5	2,5-Didehydrogluconate reductase*	WP_018633267	566	7	30,332	5.81	Ketogluconate metabolism
552	5.8	11.5	Pentapeptide repeat-containing protein*	WP_018634194	116	3	21,188	5.86	Uncharacterized
795	9.7	23.5	Membrane protein	WP_018634320	126	3	35,466	6.05	Uncharacterized

[a] The time at which the fold change listed occurred

[b] An * indicates homology-based identification of a hypothetical protein using Blastp (see Table S6 for related information)

[c] A [§] indicates a Mascot taxonomy other than *Meganema perideroedes* (see Table S5 for related information)

[d] The calculated molecular weight of the identified protein

[e] The calculated isoelectric point of the identified protein

Table 4 Identification and functional characterization of protein spots exhibiting at least a twofold change increase in abundance during the famine phase relative to the feast phase

Spot	Fold change	Time (h)[a]	Protein name[b,c]	Accession	Mascot score	Matched peptides	MW[d]	pI[e]	General function
38	5.0	11.5	Quinohemoprotein amine dehydrogenase*	WP_018634151	170	4	55,372	4.81	Energy production and conversion
69	3.3	11.5	Glycerol kinase*	WP_018632171	265	6	54,320	5.29	Energy production and conversion
469	2.3	23.5	F_0F_1 ATP synthase subunit beta	WP_018631700	313	7	50,791	4.79	Energy production and conversion
1809	3.3	11.5	Fumarate hydratase	WP_018633280	211	4	49,297	5.74	Energy generation and conversion
4746	3.4	11.5	Quinone oxidoreductase	WP_018632319	220	4	35,673	5.53	Energy production and conversion
4960	2.6	4.5	F_0F_1 ATP synthase subunit alpha§	WP_004261865	288	5	55,268	5.59	Energy production and conversion
150	2.4	4.5	Acetyl-CoA synthetase	WP_018631372	169	3	70,657	5.88	Lipid transport and metabolism
151	2.3	11.5	Acetyl-CoA acetyltransferase	WP_018631634	328	2	40,685	5.97	Lipid transport and metabolism
327	2.5	11.5	Propionyl-CoA synthetase	WP_018632631	178	4	68,489	5.73	Lipid transport and metabolism
541	9.4	11.5	Succinyl-CoA:3-ketoacid-CoA transferase	WP_018634294	100	2	22,360	4.69	Lipid transport and metabolism
11	3.4	17.5	Sulfate transporter subunit*	WP_018634284	672	7	36,835	4.91	Nutrient transport
13	2.3	23.5	ABC transporter permease	WP_018632451	533	7	42,583	4.83	Nutrient transport
37	4.6	23.5	ABC transporter substrate-binding protein*	WP_018633424	896	11	38,323	4.72	Nutrient transport
59	5.8	17.5	ABC transporter substrate-binding protein*	WP_018633424	577	9	38,323	4.72	Nutrient transport
82	3.4	23.5	ABC transporter substrate-binding protein	WP_040789902	406	7	57,296	4.80	Nutrient transport
156	2.5	23.5	ABC transporter substrate-binding protein*	WP_018631899	180	3	39,576	6.36	Nutrient transport
165	2.6	17.5	Amino acid ABC transporter*	WP_018632269	258	4	37,330	4.69	Nutrient transport
181	4.1	17.5	Amino acid ABC transporter*	WP_018632269	408	7	37,330	4.69	Nutrient transport
232	6.2	23.5	ABC transporter substrate-binding protein*	WP_018633993	339	6	33,128	4.53	Nutrient transport
236	2.8	23.5	ABC transporter substrate-binding protein*	WP_018631899	117	3	39,576	6.36	Nutrient transport
244	2.6	4.5	Amino acid ABC transporter*	WP_018632268	481	8	37,781	4.89	Nutrient transport
370	4.2	11.5	TelA*	WP_018632854	296	6	45,037	5.48	Inorganic ion transport and metabolism
75	2.8	23.5	Multifunctional 2′3′-cyclic-nucleotide 2′phosphodiesterase	WP_018631853	801	10	58,603	4.72	Nucleotide transport and metabolism
8	6.3	17.5	Molecular chaperone GroEL	WP_018633070	1441	19	57,962	5.05	Posttranslation protein modification
63	4.4	11.5	Molecular chaperone GroEL	WP_018633070	909	15	57,962	5.05	Posttranslation protein modification
218	3.4	17.5	Molecular chaperone GroEL	WP_018633070	574	8	57,962	5.05	Posttranslation protein modification
4978	5.37	11.5	Molecular chaperone GroEL	WP_018633070	265	5	57,962	5.05	Posttranslation protein modification
5837	3.9	17.5	Sigma-54-dependent Fis family transcriptional regulator	WP_018633103	80	2	53,526	5.41	Signal transduction
419	2.0	23.5	Elongation factor Tu	WP_018631570	154	2	43,422	5.42	Translation
42	2.0	23.5	Membrane protein*	WP_018633522	623	9	34,894	5.00	Uncharacterized

[a] The time at which the fold change listed occurred

[b] An * indicates homology-based identification of a hypothetical protein using Blastp (see Table S6 for related information)

[c] A § indicates a Mascot taxonomy other than *Meganema perideroedes* (see Table S5 for related information)

[d] The calculated molecular weight of the identified protein

[e] The calculated isoelectric point of the identified protein

Table 5 Identification and functional characterization of protein spots exhibiting at least a twofold change increase in abundance in the fed-batch PHA production samples compared to the SBR samples or in the SBR samples compared to the fed-batch PHA production reactor

Spot	Fold change	Protein name[a]	Accession	Mascot score	Matched peptides	MW[b]	pI[c]	General function
Fed-batch								
9	2.2	F_0F_1 ATP synthase subunit alpha	WP_018631697	139	3	55,571	5.70	Energy production and conversion
488	6.4	ATP synthase epsilon chain*	WP_018631701	177	2	13,935	4.89	Energy production and conversion
518	2.9	Methylmalonate-semialdehyde dehydrogenase*	WP_018632449	151	2	54,008	5.94	Energy production and conversion
648	5.2	Malate dehydrogenase	WP_018631935	131	2	33,324	5.49	Energy production and conversion
201	9.1	Phasin*	WP_018634051	196	3	18,623	5.80	PHA synthesis
344	2.3	Phasin*	WP_018634051	311	6	18,623	5.80	PHA synthesis
572	2.1	Phasin*	WP_018634051	334	6	18,623	5.80	PHA synthesis
1956	3.2	Phasin*	WP_018634051	486	8	18,623	5.80	PHA synthesis
46	2.0	ABC transporter substrate-binding protein*	WP_018633957	344	7	54,148	4.96	Nutrient transport
325	2.3	Molecular chaperone GroEL	WP_018633070	981	14	57,962	5.05	Posttranslation protein modification
SBR								
28	2.4	Dihydrolipoamide dehydrogenase*	WP_018632931	537	8	48,291	5.79	Energy production and conversion
81	2.8	Adenylate kinase	WP_018631593	240	4	22,738	5.46	Energy production and conversion
429	23.5	Amino acid ABC transporter substrate-binding protein	WP_018632268	366	5	37,781	4.89	Nutrient transport
257	2.1	Transcription termination/antitermination factor NusG	WP_018631560	126	3	20,049	5.16	Transcription

[a] An * indicates homology-based identification of a hypothetical protein using Blastp (see Table S6 for related information)

[b] The calculated molecular weight of the identified protein

[c] The calculated isoelectric point of the identified protein

PHA production in a fed-batch reactor was evaluated to assess the overall PHA production capacity of the enriched MMC. The maximum PHA content reached in this study (40 % wt. basis) was in the range of other studies using waste feedstocks, including tomato cannery wastewater (~20 %) (Liu et al. 2008) and fermented paper mill effluent (~48 %) (Bengtsson et al. 2008), although lower compared to other fermented feedstocks, such as molasses (~74 %) (Albuquerque et al. 2013) and paper mill wastewater (~77 %) (Jiang et al. 2012). The PHA yield in the fed-batch assessments was generally lower compared to previous studies using fermented waste feedstocks (0.62–0.80 Cmmol PHA Cmmol VFA^{-1}) (Albuquerque et al. 2013; Jiang et al. 2012); the PHA yield observed for sampling #1 (1.14 Cmmol PHA Cmmol VFA^{-1}) indicated non-VFA substrates contributed to PHA production. Though not quantified, the non-VFA readily biodegradable substrate may have included residual, unfermented substrate from the first stage (considering the original matrix was raw dairy manure, simple carbohydrates and long chain fatty acids are logical candidates). Comparing the aforementioned intracellular PHA content and production yield values reported in the literature to this research suggests further optimization of the reactors operated herein is possible. Nevertheless, the enriched MMC was a suitable candidate for the microbial community and proteomic profiling as the feast-famine response was consistently observed and the PHA production in the fed-batch reactor exceeded that in the enrichment SBR in all three sampling events.

Microbial community analysis

The microbial composition of the MMC, interrogated through high-throughput 16S rRNA gene sequencing, differed significantly at the genus level as compared with other ADF enrichment investigations. Though the most abundant genus identified in this study (*Meganema*) has been observed in another ADF enrichment SBR (Majone et al. 2006), the high abundance of *Meganema* was in contrast to other studies that more commonly reported dominant genera including *Thauera* (Albuquerque et al. 2013; Carvalho et al. 2013; Lemos et al. 2008), *Azoarcus* (Bengtsson et al. 2010a; Bengtsson et al. 2010b; Waller et al. 2012), or *Plasticicumulans* (Jiang et al. 2011; Jiang et al. 2012; Marang et al. 2013). Additionally, some of the PHA-producing genera identified in this study such as *Nannocystis*, *Hyphomonas*, and *Rhodopirellula* have not been reported in other ADF investigations involving waste feedstocks. The number of taxa identified in this study was also higher compared to previous studies, and the microbial diversity (based on the Shannon index) was higher than that reported for an ADF enrichment SBR cultivated on fermented molasses (Shannon index ≤1.0) (Carvalho et al. 2013). High-throughput DNA sequencing (i.e., a more sophisticated method as compared to FISH or DGGE DNA band sequencing)

may explain the more diverse MMC observed in this study, but other possible explanations for the dissimilarity in microbial composition include differing inoculum sources, feedstock composition, and applied operating conditions. More importantly, independent of the marked differences in microbial composition in this study relative to others, a similar feast-famine response at a bulk solution-level was observed in the SBR, indicating that the microbial composition may not be the strongest determinant in eliciting a feast-famine response. Rather, the functional capabilities of the taxa present may be more pertinent.

To explore the potential implications of the microbial composition and associated functional capabilities with respect to the bulk solution parameter observations, the major phylotypes (those comprising at least 1 % of the total abundance) during the sampling events were further scrutinized. Of note, not all phylotypes were assigned at the species level, meaning that the associated functional capabilities could not be established with certainty. However, for the sake of speculation, subordinate taxa (and their associated physiology) may be considered as surrogates in the evaluation of bulk solution changes. For example, the capabilities of the most abundant genus identified (*Meganema*) may be evaluated by considering the only species currently in the RDP database, namely *M. perideroedes*, as a proxy. *M. perideroedes* is a filamentous organism that was identified in activated sludge (Thomsen et al. 2006) and was shown to exhibit rapid substrate uptake (including acetate, propionate, and butyrate) using various electron acceptors (oxygen, nitrite, and nitrate) in addition to a high PHA accumulation capacity (Kragelund et al. 2005; Thomsen et al. 2006). These metabolic characteristics of *M. perideroedes*, coupled with the observation of more than half of the major phylotypes identified having at least one member known to possess a subset of VFA assimilation, PHA synthesis, or denitrification (at least one step), aligned with the observed bulk solution changes.

Considering the three sampling events, the maximum PHA content and PHA yield achieved in the fed-batch production assessments corresponded to the MMC composition with the lowest species richness and diversity (sampling #1), whereas the lowest maximum PHA content and PHA yield corresponded to the MMC with the highest species richness (sampling #3). Comparatively, some of the highest maximum PHA contents achieved (75–80 % PHA for waste feedstocks (Albuquerque et al. 2010; Carvalho et al. 2013) and upwards of 90 % PHB for synthetic substrates (Jiang et al. 2011; Johnson et al. 2009)) were achieved with MMC enrichments with low microbial diversity. Accordingly, lower microbial diversity in enriched MMCs may be favorable for fed-batch PHA production, particularly when increased microbial diversity is associated with more non-PHA-producing bacteria—an observation other investigations have also made (Jiang et al. 2012; Queiros et al. 2014; Tamis et al. 2014). Considering the superior microbial community characterization obtainable using high-throughput 16S rRNA gene sequencing, the tool may provide a useful means to assess and troubleshoot overall PHA process operations and performance.

Proteomic profiling

The application of proteomics to an ADF-driven system complements the pre-existing, well-established macro-level characterization of these systems by providing the protein and enzymatic-level perspective necessary to enhance associated process knowledge. Indeed, the high resolving power of 2DE coupled with LC-MS/MS permitted the evaluation of highly abundant proteins in the MMC and those exhibiting differential abundance during an SBR cycle and fed-batch PHA production. Overall, the quality of the 2DE gels and number of protein spots resolved in this study were comparable to other studies involving processes with complex MMCs, such as enhanced biological phosphorus removal (Wilmes et al. 2008) and anaerobic digestion (Hanreich et al. 2013). The numerous assignments to *M. perideroedes* substantiated the observed abundance of the genus as revealed by the 16S rRNA gene sequencing. The detection of proteins associated with other taxa may have been impeded by the lack of genome sequences available for many of the genera identified, coupled with potential biases towards proteins arising from the most abundant species in the protein extraction procedure or 2DE (Holmsgaard et al. 2011; Jehmlich et al. 2010). Nevertheless, proteins physiologically relevant to the metabolic response of the MMC to ADF conditions and PHA synthesis/degradation were identified, supporting the macro-level observations and microbial phylogenetic characterization.

Highly abundant proteins

Highly abundant protein spots shared by all gels were expected to provide insight into prominent functions in the MMC which proceeded independent of exogenous substrate availability. The consistently high abundance of porin proteins may be explained by the necessity to sustain nutrient (small molecules <1000 Da; e.g., ions, carbohydrates, peptides, signaling molecules, etc.) diffusion and transport into the cell (Koch 1990; Koch 1997; Konopka 2000), which was further supported by the high abundance of two amino acid transporters. The high abundance of superoxide dismutase throughout the SBR cycle was consistent with the need to destroy superoxide anion radicals generated under the applied aerobic conditions (White 2007). The high abundance of bacterioferritin may have contributed to the destruction of the hydrogen peroxide produced by superoxide dismutase, since these iron storage proteins exhibit ferroxidation chemistry, in addition to contributing to iron homeostasis (Chiancone et al. 2004).

Feast phase

The identification of proteins integral to PHA synthesis during the SBR feast phase corroborated the VFA uptake and PHA synthesis behavior consistently observed under ADF conditions. The increased abundance of acetyl-CoA acetyltransferase (also referred to as β-ketothiolase) was logical, as this enzyme catalyzes the first step of polyhydroxybutyrate synthesis via the condensation of two acetyl-CoA moieties to yield acetoacetyl-CoA (the precursor to HB) (Steinbüchel and Schlegel 1991). This enzyme may have also been involved in the condensation of acetyl-CoA and propionyl-CoA to yield 3-ketovaleryl-CoA (the precursor to HV). The presence of this enzyme for the entire SBR cycle (Fig. S21) was in accordance with pure culture studies reporting the enzyme's constitutive expression and involvement in other metabolic pathways (Brigham et al. 2012; Lawrence et al. 2005). In fact, a basal level of acetyl-CoA acetyltransferase at the end of the SBR cycle may be advantageous to PHA-producing bacteria, as PHA synthesis could be initiated quickly in the subsequent feast phase. Lastly, the presence of acetyl-CoA acetyltransferase coupled with the detection of peptides from NADPH-dependent acetoacetyl-CoA reductase and PHA synthase (Table S5) provides the first experimental evidence of the enzymes constituting the canonical PHA synthesis pathway in an MMC cultivated under ADF conditions, supporting the assumed similarity with pure cultures.

Also aligning with the observed PHA synthesis was the detection of multiple phasin proteins, which are non-catalytic structural proteins that envelope the surface of PHA granules (Pötter and Steinbüchel 2005). Phasins have been shown to be involved with diverse functions, including preventing PHA granule coalescence upon contact with the cytoplasm (Wieczorek et al. 1995), regulating the size and number of PHA granules (Kuchta et al. 2007) and displaying chaperone-like protection from heat and superoxide stress (Mezzina et al. 2015). Apart from roles in PHA synthesis, phasin proteins have also been shown to be involved in PHA degradation (Kuchta et al. 2007). Additionally, in pure culture investigations, distinct phasin proteins (Pötter et al. 2004; Wieczorek et al. 1995) and phasin isoforms (Smit et al. 2012) have been identified in relation to PHA synthesis. Considering some of the phasin protein spots detected in this study displayed markedly different isoelectric points, some of the phasin proteins may have been unique, potentially exhibiting differential functionality in catabolic or anabolic processes. Accordingly, phasin isoforms in the MMC may have functioned in modulating the transport of PHA monomers or oligomers across the PHA granule surface, making them available for central metabolic processes.

Additional proteins identified from the feast phase reinforced the simultaneous occurrence of PHA synthesis and growth often inferred from bulk solution parameter assessments. Specifically, the detection of enzymes involved with energy generation for growth and cellular maintenance (viz. isocitrate dehydrogenase, malate dehydrogenase, malyl-CoA lyase, and aldehyde dehydrogenase) supported the concept that carbon substrates were used for respiration concurrent with PHA synthesis (Dias et al. 2006; Reis et al. 2003). Related to cellular respiration and PHA synthesis, biochemical reactions generating reducing equivalents during the feast phase were expected to occur. Indeed, NADPH, the electron carrier supplying reducing equivalents to PHA, could have been generated by the reaction catalyzed by isocitrate dehydrogenase (isocitrate + $NADP^+ \leftrightarrow \alpha$-ketoglutarate + CO_2 + NADPH + H^+) (White 2007) as well as by the activity of 2,5-didehydrogluconate reductase (2-keto-D-gluconic acid + $NADP^+ \leftrightarrow$ 2,5-didehydro-D-gluconate + NADPH + H^+) (Khurana et al. 2000). Additionally, the detection of proteins involved in protein synthesis (viz. 50S ribosomal protein L6, elongation factor Tu, chaperone GroEL) in increased abundance during the feast phase supported biomass growth concurrent with PHA synthesis.

Finally, the detection of methylmalonate-semialdehyde dehydrogenase during the feast phase was intriguing, as this enzyme can generate acetyl-CoA and propionyl-CoA (PHBV precursors) from malonate semialdehyde and methylmalonate-semialdehyde, respectively, which are intermediates of valine degradation (Bannerjee et al. 1970). Though the presence of valine in the FDML was undetermined, PHBV synthesis has been reported for a pure culture mutant that overproduced valine in the presence of sufficient ammonia (Steinbüchel and Pieper 1992), suggesting the amino acid may be a suitable precursor for PHBV synthesis in MMCs. Accordingly, supplementing waste feedstocks with valine may offer a strategy to increase the HV content of PHA and thus improve polymer material properties (Dekoning 1995).

Famine phase

The ability to sequester exogenous nutrients while concurrently utilizing endogenous reserves to support growth and cellular maintenance during the famine phase is expected to be a critical aspect of the MMC functional response to ADF conditions. In this regard, the detection of ABC transporters in multiple discrete protein spots, many of which increased in abundance as the SBR cycle progressed (Figs. S45–S55), aligned with the use of binding protein-dependent systems for nutrient acquisition (Ferenci 1999). More specifically, exogenous amino acids may have been in decreased abundance since at least three of the assigned ABC transporters were specific for amino acids and an enzyme involved in serine biosynthesis (D-3-phosphoglycerate dehydrogenase) was detected. Beyond the value of obtaining nutrients to support growth and cellular maintenance during the famine phase,

the presence of many ABC transporters in high abundance at the end of an SBR cycle provides an additional explanation for the rapid substrate uptake in the subsequent feast phase. Previous descriptions concerning the feast phase have emphasized that PHA storage facilitates rapid substrate uptake (Johnson et al. 2009; Reis et al. 2003; van Loosdrecht et al. 1997), but the results presented herein suggest the abundance of transport proteins may also be important in facilitating rapid substrate uptake.

Another central concept concerning the functional response to ADF conditions includes the famine phase mobilization of PHA stores to support growth and cellular maintenance. The increased abundance of acetyl-CoA synthetase, propionyl-CoA synthetase, and succinyl-CoA:3-ketoacid-CoA transferase corresponded with the observed PHA depletion. As PHA was hydrolyzed, liberated PHA monomers could have been activated by the aforementioned acyl-CoA synthetases to metabolites suitable for oxidation (Ruth et al. 2008), possibly through the TCA cycle as evidenced by the detection of fumarate hydratase in increased abundance (coupled with the presence of TCA cycle enzymes identified from the feast phase, Figs. S27, S29, S30, S33). The resulting acetyl-CoA could immediately enter the TCA cycle, whereas propionyl-CoA could either enter the TCA cycle as succinyl-CoA (via methylmalonyl-CoA) or be converted to pyruvate via the methylcitrate pathway (Textor et al. 1997). The detection of succinyl-CoA:3-ketoacid-CoA transferase further supported PHA monomer utilization via the TCA cycle, as this enzyme is involved in the reversible condensation of acetoacetyl-CoA and succinate to yield succinyl-CoA and acetoacetate.

Because MMCs must respond to diminishing exogenous nutrients in ADF SBRs during the famine phase, energy generation and substrate scavenging are anticipated to be crucial functions. The necessity of generating energy during the famine phase was supported by the detection of two ATP synthase subunits, quinone oxidoreductase and aldehyde dehydrogenase, in increased abundance. Regarding substrate scavenging, the increased abundance of quinohemoprotein amine dehydrogenase, an enzyme that deaminates primary aliphatic and aromatic amines, suggested the utilization of amines as a source of carbon, nitrogen, and energy (Takagi et al. 2001). Additionally, though the detection of glycerol kinase in increased abundance was not expected (as glycerol was not anticipated to be present in the FDML), the enzyme can phosphorylate other substrates including dihydroxyacetone, D-glyceraldehyde, and L-glyceraldehyde (Hayashi and Lin 1967), which could contribute to the generation of biomass precursors, thus supporting growth.

Cellular maintenance and housekeeping functions are expected to occur during the famine phase. The detection of chaperone GroEL in increased abundance may have been partly attributed to new protein synthesis that may have occurred during the famine phase. Additionally, an increase in chaperone GroEL during the famine phase may have been in response to potential protein misfolding caused by physiological stress, as observed in another study wherein an increase in chaperone GroEL was detected in response to starvation (Patrauchan et al. 2012). Lastly, the identification of proteins involved in other housekeeping functions (e.g., transcription and DNA processing) in increased abundance supported existing descriptions of maintenance functions occurring in the famine (Albuquerque et al. 2010; Dias et al. 2006).

Fed-batch PHA production

The proteome profile for the fed-batch PHA production assessments was expected to share commonalities with the feast phase of the SBR cycle, with potential increased abundance of critical PHA synthesis-related proteins. Indeed, acetyl-CoA acetyltransferase and multiple phasin proteins were in increased abundance during the fed-batch PHA production assessments, which was in agreement with the higher PHA content achieved therein. Also similar to the feast phase proteome profile for the SBR, the detection of methylmalonate-semialdehyde dehydrogenase in increased abundance during fed-batch PHA production suggested valine may be a potentially useful substrate for fed-batch PHA production to increase PHA content and HV fraction. Comparing the SBR in its entirety to fed-batch PHA production, dihydrolipoamide dehydrogenase, adenylate kinase, and a transcription/antitermination factor were detected in increased abundance, reinforcing the activity of central metabolic pathways, energy homeostasis maintenance, and housekeeping functions in the MMC in the enrichment SBR. Additionally, the increased abundance of an amino acid transporter in the SBR indicates that amino acid transport may be less crucial during fed-batch PHA production, supporting the characterization of the fed-batch condition as an extended feast phase (section "Feast phase"). Though these four proteins provide limited insight into the differences in performance between the fed-batch and SBR, their detection does contribute to a larger perspective. Considering the proteomic results presented herein in aggregate, it is apparent that the MMC functionality under ADF conditions extends beyond the reductionist models commonly adopted. By expanding the coverage of identified proteins, the range and implications of this functional diversity may be elucidated, revealing not only the physiological differences between the ADF enrichment and PHA production conditions but also additional insight for overall process design and operation.

In conclusion, this study investigated, for the first time, the microbial community proteome of an enriched MMC as part of a multi-stage, ADF-driven PHA production system cultivated on a waste feedstock. Despite differing operating conditions and microbial community composition relative to other investigations using fermented waste feedstocks, a feast-famine

metabolic response was established in the MMC, which highlights the flexibility in implementing ADF conditions. Many of the proteins detected in this study could be directly linked to aspects of the existing conceptual descriptions of the MMC feast-famine metabolic response under ADF conditions, providing evidence in support of conventional bulk solution variable observations. In addition, new insight was gained regarding particular microbial physiological features that have generally been overlooked in the context of ADF-driven MMC PHA production. For example, the observation of several discrete phasin proteins exhibiting differential abundance during the SBR cycle and fed-batch PHA production suggested these PHA granule-bound proteins may have potentially unique roles in both MMC enrichment via ADF and PHA production. The abundance dynamics of ATP-binding dependent transport proteins during the SBR cycle underscored the significance of nutrient transport under ADF conditions, in relation to both scavenging nutrients to withstand famine conditions and facilitating rapid substrate uptake upon commencement of the subsequent feast phase. Lastly, this proteomic analysis may provide an enhanced basis from which future studies may expand. For example, particular proteins detected in this study (e.g., phasins) may be the focus of further biochemical, functional, and regulatory characterization in relation to PHA process performance. Ultimately, the enhancement of the fundamental understanding of MMC functionality under ADF and fed-batch PHA production conditions may contribute to the optimization of large-scale multi-stage PHA production schemes using waste feedstocks and MMCs.

Acknowledgments The authors acknowledge Dr. Armando McDonald at the University of Idaho for the use of GC-MS. The authors acknowledge Mr. Dan New and Dr. Alida Gerritsen at the Institute for Bioinformatics and Evolutionary Studies Genomics Resources Core at the University of Idaho, and Dr. Matt Settles at the Bioinformatics Core at the Genome Center at the University of California-Davis for the technical assistance related to the 16S rRNA gene sequencing and bioinformatics analysis. The authors acknowledge Dr. Lee Deobald at the Mass Spectrometry Core at the University of Idaho for the technical assistance related to the LC-MS/MS proteomic analysis.

Compliance with ethical standards

Funding This material is based on work supported by the National Science Foundation under Grant Number CBET-0950498, the Environmental Protection Agency Science to Achieve Results Fellowship Program, and the National Institute of General Medical Sciences from the National Institutes of Health P30 GM103324. Any opinions, findings, and conclusions or recommendations expressed in this material are those of the authors and do not necessarily reflect the views of the funding agency.

Conflict of interest The authors declare that they have no conflicts of interest.

Ethical approval This article does not contain any studies with human participants or animals performed by any of the authors.

References

Abram F, Enright AM, O'Reilly J, Botting CH, Collins G, O'Flaherty V (2011) A metaproteomic approach gives functional insights into anaerobic digestion. J Appl Microbiol 110(6):1550–1560. doi:10.1111/j.1365-2672.2011.05011.x

Albuquerque MGE, Eiroa M, Torres C, Nunes BR, Reis MAM (2007) Strategies for the development of a side stream process for polyhydroxyalkanoate (PHA) production from sugar cane molasses. J Biotechnol 130(4):411–421. doi:10.1016/j.jbiotech.2007.05.011

Albuquerque MGE, Torres CAV, Reis MAM (2010) Polyhydroxyalkanoate (PHA) production by a mixed microbial culture using sugar molasses: effect of the influent substrate concentration on culture selection. Water Res 44(11):3419–3433. doi:10.1016/j.watres.2010.03.021

Albuquerque MGE, Carvalho G, Kragelund C, Silva AF, Crespo MTB, Reis MAM, Nielsen PH (2013) Link between microbial composition and carbon substrate-uptake preferences in a PHA-storing community. ISME J 7(1):1–12. doi:10.1038/ismej.2012.74

Bannerjee D, Sanders LE, Sokatch JR (1970) Properties of purified methylmalonate semialdehyde dehydrogenase of *Pseudomonas aeruginosa*. J Biol Chem 245(7):1828–1835

Bansal R, Deobald LA, Crawford RL, Paszczynski AJ (2009) Proteomic detection of proteins involved in perchlorate and chlorate metabolism. Biodegradation 20(5):603–620. doi:10.1007/s10532-009-9248-0

Bengtsson S, Werker A, Christensson M, Welander T (2008) Production of polyhydroxyalkanoates by activated sludge treating a paper mill wastewater. Bioresour Technol 99(3):509–516. doi:10.1016/j.biortech.2007.01.020

Bengtsson S, Pisco AR, Johansson P, Lemos PC, Reis MAM (2010a) Molecular weight and thermal properties of polyhydroxyalkanoates produced from fermented sugar molasses by open mixed cultures. J Biotechnol 147(3–4):172–179. doi:10.1016/j.jbiotec.2010.03.022

Bengtsson S, Pisco AR, Reis MAM, Lemos PC (2010b) Production of polyhydroxyalkanoates from fermented sugar cane molasses by a mixed culture enriched in glycogen accumulating organisms. J Biotechnol 145(3):253–263. doi:10.1016/j.jbiotec.2009.11.016

Beun JJ, Dircks K, Van Loosdrecht MCM, Heijnen JJ (2002) Poly-β-hydroxybutyrate metabolism in dynamically fed mixed microbial cultures. Water Res 36(5):1167–1180. doi:10.1016/S0043-1354(01)00317-7

Brigham CJ, Speth DR, Rha C, Sinskey AJ (2012) Whole-genome microarray and gene deletion studies reveal regulation of the polyhydroxyalkanoate production cycle by the stringent response in *Ralstonia eutropha* H16. Appl Environ Microbiol 78(22):8033–8044. doi:10.1128/aem.01693-12

Carvalho G, Oehmen A, Albuquerque MG, Reis MA (2013) The relationship between mixed microbial culture composition and PHA production performance from fermented molasses. New Biotechnol. doi:10.1016/j.nbt.2013.08.010

Checinska A, Burbank M, Paszczynski AJ (2012) Protection of *Bacillus pumilus* spores by catalases. Appl Environ Microbiol 78(18):6413–6422. doi:10.1128/aem.01211-12

Chiancone E, Ceci P, Ilari A, Ribacchi F, Stefanini S (2004) Iron and proteins for iron storage and detoxification. Biometals 17(3):197–202. doi:10.1023/B:BIOM.0000027692.24395.76

Coats ER, Gregg M, Crawford RL (2011) Effect of organic loading and retention time on dairy manure fermentation. Bioresour Technol 102(3):2572–2577. doi:10.1016/j.biortech.2010.11.108

Dai J, Gliniewicz K, Settles ML, Coats ER, McDonald AG (2015) Influence of organic loading rate and solid retention time on polyhydroxybutyrate production from hybrid poplar hydrolysates using mixed microbial cultures. Bioresour Technol 175:23–33. doi:10.1016/j.biortech.2014.10.049

Dekoning G (1995) Physical-properties of bacterial poly((R)-3-hydroxyalkanoates). Can J Microbiol 41:303–309. doi:10.1139/m95-201

Dias JM, Lemos PC, Serafim LS, Oliveira C, Eiroa M, Albuquerque MG, Ramos AM, Oliveira R, Reis MA (2006) Recent advances in polyhydroxyalkanoate production by mixed aerobic cultures: from the substrate to the final product. Macromol Biosci 6(11):885–906. doi:10.1002/mabi.200600112

DiGregorio BE (2009) Biobased performance bioplastic: Mirel. Chem Biol 16(1):1–2. doi:10.1016/j.chembiol.2009.01.001

Dionisi D, Majone M, Papa V, Beccari M (2004) Biodegradable polymers from organic acids by using activated sludge enriched by aerobic periodic feeding. Biotechnol Bioeng 85(6):569–579. doi:10.1002/bit.10910

Dionisi D, Carucci G, Papini MP, Riccardi C, Majone M, Carrasco F (2005) Olive oil mill effluents as a feedstock for production of biodegradable polymers. Water Res 39(10):2076–2084. doi:10.1016/j.watres.2005.03.011

Dobroth ZT, Hu S, Coats ER, McDonald AG (2011) Polyhydroxybutyrate synthesis on biodiesel wastewater using mixed microbial consortia. Bioresour Technol 102(3):3352–3359. doi:10.1016/j.biortech.2010.11.053

Eaton AD, Clesceri LS, Rice EW, Greenberg AE (2005) Standard methods for the examination of water & wastewater. 21st ed

Ferenci T (1999) Regulation by nutrient limitation. Curr Opin Microbiol 2(2):208–213. doi:10.1016/S1369-5274(99)80036-8

Hanreich A, Schimpf U, Zakrzewski M, Schlueter A, Benndorf D, Heyer R, Rapp E, Puehler A, Reichl U, Klocke M (2013) Metagenome and metaproteome analyses of microbial communities in mesophilic biogas-producing anaerobic batch fermentations indicate concerted plant carbohydrate degradation. Syst Appl Microbiol 36(5):330–338. doi:10.1016/j.syapm.2013.03.006

Hanson AJ, Paszczynski AJ, Coats ER (2016) Proteomic profiling of an undefined microbial consortium cultured in fermented dairy manure: methods development. Electrophoresis:n/a-n/a. doi:10.1002/elps.201500400

Hayashi S-I, Lin ECC (1967) Purification and properties of glycerol kinase from *Escherichia coli*. J Biol Chem 242(5):1030–1035

Henze M, Gujer W, Mino T, Matsuo T, Wentzel MC, Marais GR (1995) Wastewater and biomass characterization for the Activated Sludge Model No. 2: biological phosphorus removal. Water Sci Technol 31(2):13–23. doi:10.1016/0273-1223(95)00176-N

Hill TCJ, Walsh KA, Harris JA, Moffett BF (2003) Using ecological diversity measures with bacterial communities. FEMS Microbiol Ecol 43(1):1–11. doi:10.1111/j.1574-6941.2003.tb01040.x

Holmsgaard PN, Norman A, Hede SC, Poulsen PHB, Al-Soud WA, Hansen LH, Sørensen SJ (2011) Bias in bacterial diversity as a result of Nycodenz extraction from bulk soil. Soil Biol Biochem 43(10):2152–2159. doi:10.1016/j.soilbio.2011.06.019

Jehmlich N, Kleinsteuber S, Vogt C, Benndorf D, Harms H, Schmidt F, von Bergen M, Seifert J (2010) Phylogenetic and proteomic analysis of an anaerobic toluene-degrading community. J Appl Microbiol 109(6):1937–1945. doi:10.1111/j.1365-2672.2010.04823.x

Jiang Y, Marang L, Kleerebezem R, Muyzer G, van Loosdrecht MCM (2011) Polyhydroxybutyrate production from lactate using a mixed microbial culture. Biotechnol Bioeng 108(9):2022–2035. doi:10.1002/bit.23148

Jiang Y, Marang L, Tamis J, van Loosdrecht MCM, Dijkman H, Kleerebezem R (2012) Waste to resource: converting paper mill wastewater to bioplastic. Water Res 46(17):5517–5530. doi:10.1016/j.watres.2012.07.028

Johnson K, Jiang Y, Kleerebezem R, Muyzer G, van Loosdrecht MCM (2009) Enrichment of a mixed bacterial culture with a high polyhydroxyalkanoate storage capacity. Biomacromolecules 10(4):670–676. doi:10.1021/bm8013796

Keshavarz T, Roy I (2010) Polyhydroxyalkanoates: bioplastics with a green agenda. Curr Opin Microbiol 13(3):321–326. doi:10.1016/j.mib.2010.02.006

Khurana S, Sanli G, Powers DB, Anderson S, Blaber M (2000) Molecular modeling of substrate binding in wild-type and mutant *Corynebacteria* 2,5-diketo-D-gluconate reductases. Proteins 39(1):68–75. doi:10.1002/(SICI)1097-0134(20000401)39:1<68::AID-PROT7>3.0.CO;2-Y

Koch A (1990) Diffusion The crucial process in many aspects of the biology of bacteria. In: Marshall KC (ed) Advances in microbial ecology. Advances in microbial ecology, vol 11. Springer US, pp 37–70

Koch AL (1997) Microbial physiology and ecology of slow growth. Microbiol Mol Biol R 61(3):305–318

Konopka A (2000) Microbial physiological state at low growth rate in natural and engineered ecosystems. Curr Opin Microbiol 3(3):244–247. doi:10.1016/S1369-5274(00)00083-7

Kragelund C, Nielsen JL, Thomsen TR, Nielsen PH (2005) Ecophysiology of the filamentous Alphaproteobaeterium *Meganema perideroedes* in activated sludge. FEMS Microbiol Ecol 54(1):111–122. doi:10.1016/j.femsec.2005.03.002

Kuchta K, Chi L, Fuchs H, Poetter M, Steinbuechel A (2007) Studies on the influence of phasins on accumulation and degradation of PHB and nanostructure of PHB granules in *Ralstonia eutropha* H16. Biomacromolecules 8(2):657–662. doi:10.1021/bm060912e

Kuhn R, Benndorf D, Rapp E, Reichl U, Palese LL, Pollice A (2011) Metaproteome analysis of sewage sludge from membrane bioreactors. Proteomics 11(13):2738–2744. doi:10.1002/pmic.201000590

Lawrence AG, Schoenheit J, He A, Tian J, Liu P, Stubbe J, Sinskey AJ (2005) Transcriptional analysis of *Ralstonia eutropha* genes related to poly-(R)-3-hydroxybutyrate homeostasis during batch fermentation. Appl Microbiol Biotechnol 68(5):663–672. doi:10.1007/s00253-005-1969-3

Lemos PC, Levantesi C, Serafim LS, Rossetti S, Reis MAM, Tandoi V (2008) Microbial characterisation of polyhydroxyalkanoates storing populations selected under different operating conditions using a cell-sorting RT-PCR approach. Appl Microbiol Biotechnol 78(2):351–360. doi:10.1007/s00253-007-1301-5

Liang S, Gliniewicz K, Mendes-Soares H, Settles ML, Forney LJ, Coats ER, McDonald AG (2015) Comparative analysis of microbial community of novel lactic acid fermentation inoculated with different undefined mixed cultures. Bioresour Technol 179:268–274. doi:10.1016/j.biortech.2014.12.032

Liu H-Y, Hall PV, Darby JL, Coats ER, Green PG, Thompson DE, Loge FJ (2008) Production of polyhydroxyalkanoate during treatment of tomato cannery wastewater. Water Environ Res 80(4):367–372. doi:10.2175/106143007x221535

Magoč T, Salzberg SL (2011) FLASH: fast length adjustment of short reads to improve genome assemblies. Bioinformatics 27(21):2957–2963. doi:10.1093/bioinformatics/btr507

Majone M, Massanisso P, Carucci A, Lindrea K, Tandoi V (1996) Influence of storage on kinetic selection to control aerobic filamentous bulking. Water Sci Technol 34(5–6):223–232. doi:10.1016/0273-1223(96)00649-x

Majone M, Beccari M, Di Gregorio S, Dionisi D, Vallini G (2006) Enrichment of activated sludge in a sequencing batch reactor for polyhydroxyalkanoate production. Water Sci Technol 54(1):119–128. doi:10.2166/wst.2006.379

Marang L, Jiang Y, van Loosdrecht MCM, Kleerebezem R (2013) Butyrate as preferred substrate for polyhydroxybutyrate production. Bioresour Technol 142:232–239. doi:10.1016/j.biortech.2013.05.031

Mezzina MP, Wetzler DE, Almeida A, Dinjaski N, Prieto MA, Pettinari MJ (2015) A phasin with extra talents: a polyhydroxyalkanoate granule-associated protein has chaperone activity. Environ Microbiol 17(5):1765–1776. doi:10.1111/1462-2920.12636

Morgan-Sagastume F, Karlsson A, Johansson P, Pratt S, Boon N, Lant P, Werker A (2010) Production of polyhydroxyalkanoates in open,

mixed cultures from a waste sludge stream containing high levels of soluble organics, nitrogen and phosphorus. Water Res 44(18):5196–5211. doi:10.1016/j.watres.2010.06.043

Oehmen A, Pinto FV, Silva V, Albuquerque MGE, Reis MAM (2014) The impact of pH control on the volumetric productivity of mixed culture PHA production from fermented molasses. Eng Life Sci 14(2):143–152. doi:10.1002/elsc.201200220

Patrauchan MA, Miyazawa D, LeBlanc JC, Aiga C, Florizone C, Dosanjh M, Davies J, Eltis LD, Mohn WW (2012) Proteomic analysis of survival of *Rhodococcus jostii* RHA1 during carbon starvation. Appl Environ Microbiol 78(18):6714–6725. doi:10.1128/AEM.01293-12

Pötter M, Steinbüchel A (2005) Poly(3-hydroxybutyrate) granule-associated proteins: impacts on poly(3-hydroxybutyrate) synthesis and degradation. Biomacromolecules 6(2):552–560. doi:10.1021/bm049401n

Pötter M, Müller H, Reinecke F, Wieczorek R, Fricke F, Bowien B, Friedrich B, Steinbüchel A (2004) The complex structure of polyhydroxybutyrate (PHB) granules: four orthologous and paralogous phasins occur in *Ralstonia eutropha*. Microbiology 150(Pt 7):2301–2311. doi:10.1099/mic.0.26970-0

Queiros D, Rossetti S, Serafim LS (2014) PHA production by mixed cultures: a way to valorize wastes from pulp industry. Bioresour Technol 157:197–205. doi:10.1016/j.biortech.2014.01.099

Reis MAM, Serafim LS, Lemos PC, Ramos AM, Aguiar FR, Van Loosdrecht MCM (2003) Production of polyhydroxyalkanoates by mixed microbial cultures. Bioproc Biosyst Eng 25(6):377–385. doi:10.1007/s00449-003-0322-4

Roels JA (1983) Energetics and kinetics in biotechnology. Elsevier Biomedical Press, Amsterdam

Ruth K, de Roo G, Egli T, Ren Q (2008) Identification of two acyl-CoA synthetases from *Pseudomonas putida* GPo1: one is located at the surface of polyhydroxyalkanoates granules. Biomacromolecules 9(6):1652–1659. doi:10.1021/bm8001655

Serafim LS, Lemos PC, Oliveira R, Reis MAM (2004) Optimization of polyhydroxybutyrate production by mixed cultures submitted to aerobic dynamic feeding conditions. Biotechnol Bioeng 87(2):145–160. doi:10.1002/bit.20085

Serafim LS, Lemos PC, Albuquerque MGE, Reis MAM (2008) Strategies for PHA production by mixed cultures and renewable waste materials. Appl Microbiol Biotechnol 81(4):615–628. doi:10.1007/s00253-008-1757-y

Shevchenko A, Tomas H, Havlis J, Olsen JV, Mann M (2006) In-gel digestion for mass spectrometric characterization of proteins and proteomes. Nat Protoc 1(6):2856–2860. doi:10.1038/nprot.2006.468

Smit AM, Strabala TJ, Peng L, Rawson P, Lloyd-Jones G, Jordan TW (2012) Proteomic phenotyping of *Novosphingobium nitrogenifigens* reveals a robust capacity for simultaneous nitrogen fixation, polyhydroxyalkanoate production, and resistance to reactive oxygen species. Appl Environ Microbiol 78(14):4802–4815. doi:10.1128/AEM.00274-12

Steinbüchel A, Pieper U (1992) Production of a copolyester of 3-hydroxybutyric acid and 3-hydroxyvaleric acid from single unrelated carbon sources by a mutant of *Alcaligenes eutrophus*. Appl Microbiol Biotechnol 37(1):1–6. doi:10.1007/BF00174193

Steinbüchel A, Schlegel HG (1991) Physiology and molecular genetics of poly(β-hydroxyalkanoic acid) synthesis in *Alcaligenes eutrophus*. Mol Microbiol 5(3):535–542. doi:10.1111/j.1365-2958.1991.tb00725.x

Stowe EJ, Coats ER, Brinkman CK (2015) Dairy manure resource recovery utilizing two-stage anaerobic digestion—implications of solids fractionation. Bioresour Technol 198:237–245. doi:10.1016/j.biortech.2015.09.017

Takagi K, Yamamoto K, Kano K, Ikeda T (2001) New pathway of amine oxidation respiratory chain of *Paracoccus denitrificans* IFO 12442. Eur J Biochem 268(2):470–476. doi:10.1046/j.1432-1033.2001.01912.x

Tamis J, Lužkov K, Jiang Y, van Loosdrecht MC, Kleerebezem R (2014) Enrichment of *Plasticicumulans acidivorans* at pilot-scale for PHA production on industrial wastewater. J Biotechnol 192:161–169. doi:10.1016/j.jbiotec.2014.10.022

Textor S, Wendisch VF, De Graaf AA, Muller U, Linder MI, Linder D, Buckel W (1997) Propionate oxidation in *Escherichia coli*: evidence for operation of a methylcitrate cycle in bacteria. Arch Microbiol 168(5):428–436. doi:10.1007/s002030050518

Thiede B, Koehler CJ, Strozynski M, Treumann A, Stein R, Zimny-Arndt U, Schmid M, Jungblut PR (2013) High resolution quantitative proteomics of HeLa cells protein species using stable isotope labeling with amino acids in cell culture(SILAC), two-dimensional gel electrophoresis(2DE) and nano-liquid chromatograpohy coupled to an LTQ-OrbitrapMass spectrometer. Mol Cell Proteomics 12(2):529–538. doi:10.1074/mcp.M112.019372

Thomsen TR, Blackall LL, de Muro MA, Nielsen JL, Nielsen PH (2006) *Meganema perideroedes* gen. nov., sp nov., a filamentous alphaproteobacterium from activated sludge. Int J Syst Evol Micr 56:1865–1868. doi:10.1099/ijs.0.02916-0

van Loosdrecht MCM, Pot MA, Heijnen JJ (1997) Importance of bacterial storage polymers in bioprocesses. Water Sci Technol 35(1):41–47. doi:10.1016/s0273-1223(96)00877-3

VerBerkmoes NC, Denef VJ, Hettich RL, Banfield JF (2009) Systems biology: functional analysis of natural microbial consortia using community proteomics. Nat Rev Microbiol 7(3):196–205. doi:10.1038/nrmicro2080

Vizcaino JA, Cote RG, Csordas A, Dianes JA, Fabregat A, Foster JM, Griss J, Alpi E, Birim M, Contell J, O'Kelly G, Schoenegger A, Ovelleiro D, Perez-Riverol Y, Reisinger F, Rios D, Wang R, Hermjakob H (2013) The PRoteomics IDEntifications (PRIDE) database and associated tools: status in 2013. Nucleic Acids Res 41(Database issue):D1063–D1069. doi:10.1093/nar/gks1262

Waller JL, Green PG, Loge FJ (2012) Mixed-culture polyhydroxyalkanoate production from olive oil mill pomace. Bioresour Technol 120:285–289. doi:10.1016/j.biortech.2012.06.024

Wang Q, Garrity GM, Tiedje JM, Cole JR (2007) Naïve Bayesian classifier for rapid assignment of rRNA sequences into the new bacterial taxonomy. Appl Environ Microbiol 73(16):5261–5267. doi:10.1128/aem.00062-07

White D (2007) The Physiology and Biochemistry of Prokaryotes, 3rd edn. Oxford University Press

Wieczorek R, Pries A, Steinbüchel A, Mayer F (1995) Analysis of a 24-kilodalton protein associated with the polyhydroxyalkanoic acid granules in *Alcaligenes eutrophus*. J Bacteriol 177(9):2425–2435

Wilmes P, Bond PL (2004) The application of two-dimensional polyacrylamide gel electrophoresis and downstream analyses to a mixed community of prokaryotic microorganisms. Environ Microbiol 6(9):911–920. doi:10.1111/j.1462-2920.2004.00687.x

Wilmes P, Bond PL (2009) Microbial community proteomics: elucidating the catalysts and metabolic mechanisms that drive the Earth's biogeochemical cycles. Curr Opin Microbiol 12(3):310–317. doi:10.1016/j.mib.2009.03.004

Wilmes P, Wexler M, Bond PL (2008) Metaproteomics provides functional insight into activated sludge wastewater treatment. PLoS One 3(3):e1778. doi:10.1371/journal.pone.0001778

Zhou Z, Meng F, He X, Chae SR, An Y, Jia X (2015) Metaproteomic analysis of biocake proteins to understand membrane fouling in a submerged membrane bioreactor. Environ Sci Technol 49(2):1068–1077. doi:10.1021/es504489r